Mechanism and kinetics of ethanol-acetaldehyde conversion to 1,3-butadiene over isolated La Lewis acid sites in silanol nests in dealuminated Beta zeolite

Yanfei Zhang[1,2,3,4⊥], Liang Qi[2,3,4⊥], Yuting Li[5], Tingshu Yang[1], Debora M. Meira[6], Chaochao Dun[7], Haocheng Hu[3], Huihui Chen[3], Shutao Xu[3], Jeffrey J. Urban[7], Aaron D. Sadow[5,8], Takeshi Kobayashi[5], Long Qi[5], Peng Tian[3], Alexis T. Bell[2,4]*

[1] Green Shipping and Carbon Neutrality Lab, College of Environmental Science and Engineering, Dalian Maritime University, Dalian 116026, China

[2] Chemical Sciences Division, Lawrence Berkeley National Laboratory, Berkeley, California 94720, United States

[3] National Engineering Laboratory for Methanol to Olefins, Dalian National Laboratory for Clean Energy, Dalian Institute of Chemical Physics, Chinese Academy of Sciences, Dalian 116023, China.

[4] Department of Chemical and Biomolecular Engineering, University of California, Berkeley, Berkeley, California 94720, United States

[5] U.S. DOE Ames National Laboratory, Iowa State University, Ames, Iowa 50011, United States

[6] Canadian Light Source, 44 Innovation Blvd., Saskatoon, Saskatchewan S7N 2V3, Canada

[7] The Molecular Foundry, Lawrence Berkeley National Laboratory, Berkeley, CA, 94720, United States

[8] Department of Chemistry, Iowa State University, Ames, Iowa 50011, United States

⊥Contributed equally

*Correspondence to: alexbell@berkeley.edu (A. T. Bell)

Abstract

Biomass-derived ethanol (EtOH) and acetaldehyde (AcH) conversion to 1,3-butadiene (1,3-BD) is an alternative process for 1,3-BD production. The present investigation reports the preparation and characterization of isolated La sites introduced into the silanol nests in DeAlBEA as well as detailed studies of the mechanism and kinetics for conversion of an ethanol-AcH mixture to 1,3-BD. La sites supported on DeAlBEA are found to be present as $(\equiv SiO)_2La{-}OH$ groups that are H-bonded with adjacent Si-OH groups, possessing high C-C coupling activity and stability, superior to state-of-the-art Y-DeAlBEA. La sites supported silica (La-SiO_2) with similar chemical structure but no H-bonding interaction with Si-OH groups were prepared for comparison. Lewis acid La sites promote AcH aldol condensation and the activity of such sites is nearly identical for both La-DeAlBEA and La-SiO_2. The rate of C_4 products formation increases by a factor of 4.8 upon addition of EtOH to the feed of AcH over La-DeAlBEA, whereas that over La/SiO_2 remains unchanged. Investigation of the mechanism and kinetics of AcH aldol condensation and ethanol-AcH conversion to 1,3-BD revealed two C-C bond forming pathways – AcH aldol condensation by Lewis acid La sites and direct coupling of EtOH-AcH over H-bonded $(\equiv SiO)_2La{-}OH\cdots HO{-}Si\equiv$ sites. This study provides important information about the role of local environment of isolated Lewis acid sites and their effects on the direct coupling of EtOH and AcH to form 1,3-BD.

Keywords: Isolated La sites; Ethanol-acetaldehyde conversion to 1,3-butadiene; C-C coupling; Hydrogen-bonding interaction; Reaction mechanism; Kinetics

Introduction

1,3-Butadiene (1,3-BD) is a monomer for synthetic rubber and other polymers.[1-3] Today, about 95% of the global 1,3-BD is derived as a side product of naphtha steam cracking process in which ethene as the main product.[4, 5] However, due to the shift from naphtha cracking to direct dehydrogenation of light alkanes (from shale gas) to produce ethene and propene, the supply of 1,3-BD is increasingly threatened.[6] For this reason, the conversion of ethanol-to-butadiene (ETB) using bioethanol has received considerable recent attention.[1, 3, 7-11] The rapid commercialization of coal to ethanol in China has also motivated interests in ethanol upgrading processes.[12, 13]

The production of 1,3-BD from ethanol was first reported in 1900s via two routes – the one-step (Lebedev) and the two-step (Ostromisslensky) processes, both of which were commericalied.[7] Both ETB processes are proposed to proceed by similar reaction pathways: (i) EtOH dehydrogenation to AcH; (ii) aldol condensation of AcH to produce acetaldol; (iii) rapid acetaldol dehydration to form crotonaldehyde; (iv) Meerwein-Ponndorf-Verley (MPV) reduction of crotonaldehyde with EtOH to generate equal amounts of crotyl alcohol and AcH, which can participate step (ii); and (v) crotyl alcohol dehydration to produce 1,3-BD.[9, 14] Within this complex network, the formation of C-C bonds between C_2 reactants (AcH and EtOH) is the critical step for generation of 1,3-BD.

Research during the last two decades has shown that the mechanism of C-C bond formation depends critically on the composition and structure of the catalytically active centers.[1, 3, 15-19] Silica-supported transition-metal Lewis acids and magnesia-silica mixed oxides catalysts have been reported to be active for C-C bond formation, the former class of catalyst exhibiting higher activity.[1, 7] Considerable attention has been devoted recently to investigating various transition metal cations as catalysts for the ETB reaction.[7, 20-25] Supported Zr,[26, 27] Nb,[28, 29] Hf[25], Ta[30] and La[31] exhibit good activity for C-C coupling and are regarded as active centers for the EtOH-AcH conversion to 1,3-BD. The composition of the support to which Lewis acid sites are grafted also plays an important roles in ETB catalysis. The C-C coupling activity of

Lewis acid sites can be enhanced remarkably when the support is changed from amorphous silica to a siliceous zeolites.[3, 7, 15, 31, 32] Under similar reaction conditions, Ag/ZrO_2 supported on dealuminated Beta (DeAlBEA) zeolite is four times more active than $Ag/ZrO_2/SiO_2$.[33] We have recently reported that the rate of 1,3-BD formation at 573 K was about 70 times higher when isolated Lewis acid Y sites were incorporated into the silanol nests of DeAlBEA zeolite, compared with Y supported on amorphous silica.[3] The superior activity of Y/DeAlBEA was ascribed to hydrogen (H)-bonding between the -OH group of $(\equiv SiO)_2Y{-}OH$ and adjacent $\equiv Si{-}OH$ present in silanol nests of DeAlBEA. Such interactions are not present when Y is supported on silica. A similar promoting effect was also found for acetone condensation to isobutene over grafted Hf sites with and without H-bonding interaction between adjacent silanol groups.[34] Active sites having the structure of $(\equiv SiO)_3Hf{-}OH\cdots HO{-}Si\equiv$ were 4.5 times more active for C-C coupling compared to $(\equiv SiO)_3Hf{-}OH$. More recently, Li et al. have also found that C-C coupling occurs more rapidly over Lewis acid Y sites incorporated into DeAlBEA compared with Y supported on silica and deboronated MWW, the higher activity of the former catalyst was ascribed to the higher density of Lewis-acidic Y sites sites.[32]

While the importance of Lewis acid catalysts for C-C coupling has been recognized, the intrinsic role of the local structure of active sites and influence of support materials on its performance remains unclear. To date, the only consensus is that tri-, quadra-, and pentavalent metals, e.g., Y[3], La[31], Zr,[26, 27] Hf[25], Nb,[28, 29] and Ta[30] present in open $(Si\text{-}O\text{-}M^{n+})_{n-1}\text{-}OH$ sites are generally more active for C-C coupling than closed ($(Si\text{-}O\text{-}M^{n+})_n$) sites.[18, 24, 35-38] The mechanistic recognition of the influence of interactions between open-structure Lewis acid sites and characteristic groups of supports (Si-OH groups) has rarely been reported. To this point, trivalent metals such as Y/La/Ce are of particular interest because of their very high C-C coupling activity once introduced into zeolite silanol nests. However, development of a fundamental understanding of the structure-performance relationship for Y/La/Ce catalyzed ETB process has been hindered by the absence of knowledge about the interactions of

Lewis acid centers with their environment and difficulties in relating this information to the ETB reaction network.[14, 17, 18, 39, 40] Prior investigation of Lewis acid catalyzed ETB have generally considered AcH aldol condensation to be the key step in C-C bond formation; however, serious catalyst deactivation made it difficult to investigate the reaction mechanism and kinetics.

In the work reported here, we have developed a comprehensive understanding of the reaction mechanism and kinetics for the formation of 1,3-BD via aldol condensation of AcH and by condensation of AcH and EtOH. Lewis acid La exhibited high C-C coupling activity, and because this activity was stable, it enabled measurement of the kinetics of 1,3-BD formation via both processes. The structure of isolated La introduced into the silanol nest of DeAlBEA was established to be $(\equiv SiO)_2La{-}OH{\cdots}HO{-}Si\equiv$, which was confirmed using infrared spectroscopy of hydroxyl groups and adsorbed pyridine, deuterated acetonitrile, and 2,6-di-*tert*-butylpyridine, and X-ray adsorption spectroscopy (XAS). To clarify the intrinsic influence of the support silanol groups, La was grafted onto silica for comparison. This catalyst exhibited lower activity for EtOH-AcH conversion to 1,3-BD compared to La-DeAlBEA. Silica-supported La sites were formed with structure of $(\equiv SiO)_2La{-}OH$, but with no evidence for H-bonding of this species with neighboring silanol groups. The two types of isolated La sites exhibited almost identical aldol condensation activity, indicating the presence of H-bonding interaction assisted new C-C bond formation mechanism over La-DeAlBEA. The mechanism and kinetics of C-C bond formation were investigated over $(\equiv SiO)_2La{-}OH{\cdots}HO{-}Si\equiv$. It was found that the kinetic of C-C bond formation depended on the local environment of the La site. Two distinct C-C bonds formation pathways were identified – AcH aldol condensation over Lewis acid La centers and direct coupling of EtOH and AcH over H-bonded $(\equiv SiO)_2La{-}OH{\cdots}HO{-}Si\equiv$ centers, the kinetics of the latter pathway being elucidated in the present study for the first time.

Results and discussion

Catalyst characterization

The generation of silanol nests upon dealumination was evidenced by IR spectra of surface hydroxyl groups and adsorbed pyridine for H-BEA and DeAlBEA. The IR spectrum of H-BEA presented in Figure S1A exhibits a sharp band at 3743 cm^{-1} corresponding to isolated silanol (Si-OH) groups, a band at 3606 cm^{-1} corresponding to the stretching vibration of Brønsted acid Al-OH groups, and two bands at 3660 and 3780 cm^{-1} corresponding to hydroxyl groups associated with extra-framework Al species.[41-43] After dealumination, all Al-related IR bands disappear, accompanied by the appearance of a broad band centered at around 3520 cm^{-1} attributed to silanol nests in which the ≡Si-OH groups are H-bonded.[44] It is also observed that the center of the IR band for isolated silanol groups shifts to 3732 cm^{-1}, likely due to the generation of internal silanol groups.[42] Figure S1B presents IR spectra of pyridine adsorbed on H-BEA and DeAlBEA. For DeAlBEA, all of these IR bands for pyridine interacting with Brønsted and Lewis acid sites (1637, 1545, 1490, 1620 and 1453 cm^{-1}) are absent and instead two intense bands appear at 1592 and 1445 cm^{-1} due to adsorption of pyridine on H-bonded silanol nests.[3, 31, 34, 45] These changes suggest that silanol nests are created upon dealumination.

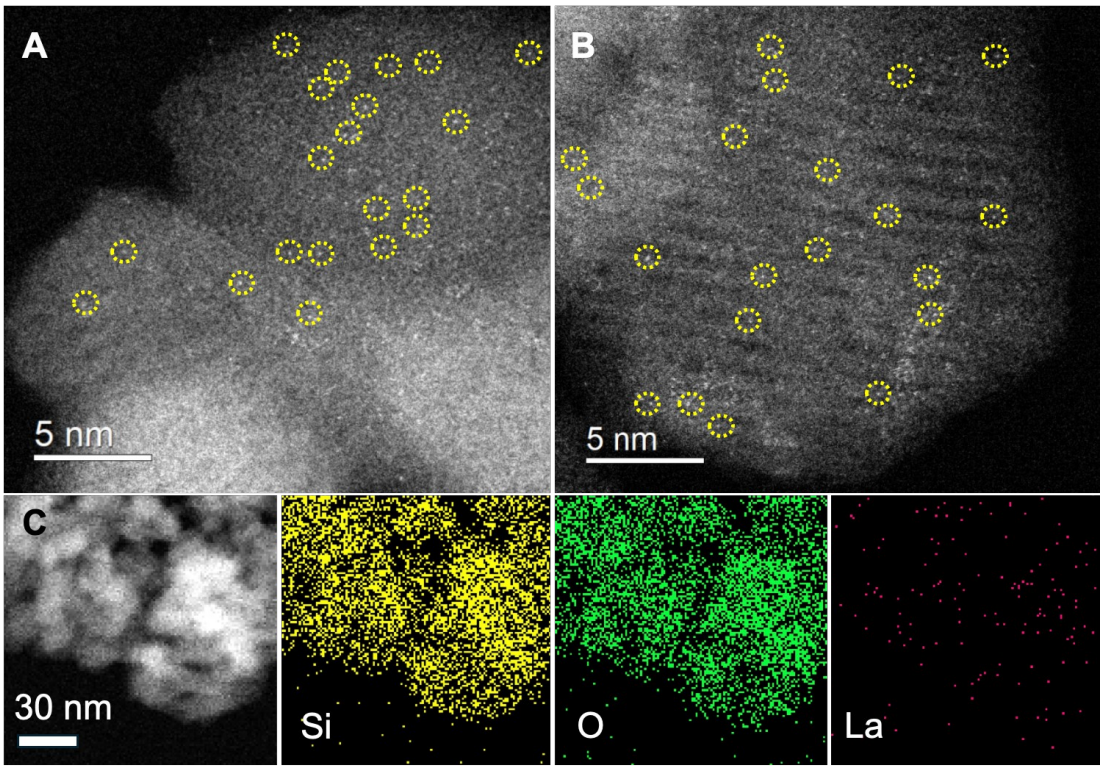

Figure 1. (A, B) The atomic-resolution Cs-corrected, high-angle annular dark field scanning transmission electron microscopy (HAADF-STEM) images (hite dots representing La atoms are outlined by yellow dashed circles) and (B) energy-dispersive X-ray mappings of 0.12La-DeAlBEA.

La was introduced to DeAlBEA zeolite by wet impregnation. ICP-OES analysis (Figure S2) shows near quantitative introduction of La, confirming the effectiveness of the strategy used to incorporate La onto DeAlBEA. XRD patterns of La-supported dealuminated Beta samples (Figure S3) exhibit identical characteristic peaks of BEA, indicating preservation of the zeolite framework upon La incorporation.[3, 41, 42, 44] No diffraction peaks for bulk La_2O_3 are observable for materials with a La/Al ratio up to 0.60, suggesting high dispersion of La species and the absence of XRD detectable metal oxide nanoparticle. To identify the detailed dispersion of La sites supported over DeAlBEA, atomic resolution Cs-corrected HAADF-STEM measurements were conducted for 0.12La-DeAlBEA. Figures 1A and 1B clearly show evidence for isolated La atoms and no evidence for small clusters of LaOx species, suggesting the La is atomically dispersed. Figure 1B shows lattice fringes with consistent orientations over the entire zeolite crystal. Additionally, energy-dispersive X-ray

(EDX) spectral mappings further reveal that the La atoms are highly and homogeneously dispersed throughout the BEA (Figure 1C).

Changes in surface hydroxyl groups were observed upon introduction of La into DeAlBEA. As shown in Figure 2A, the intensities of broad IR bands centered at around 3520 cm^{-1} decrease significantly, indicating that La is grafted into the silanol nests of the DeAlBEA likely via the formation of Si-O-La linkages.[42] Moreover, the observed attenuation of the IR band at around 3732 cm^{-1} indicates that internal silanol groups are also involved in the grafting of La species. IR spectra of adsorbed pyridine were acquired to explore the acid properties of La-DeAlBEA. Consistent with previous studies for metal-substituted zeolite materials,[32, 46] La-DeAlBEA exhibits IR bands for pyridine interacting primarily with Lewis acid centers as evidenced in Figure 2B by the appearance of a band at 1599 cm^{-1}. A significant decrease in the intensity of the signal for H-bonded pyridine at 1592 cm^{-1} is also observed that is attributed to the consumption of silanol nests during the grafting of La.[20] Because of band overlap, the IR band in the region of 1440-1460 cm^{-1} associated with pyridine adsorption on Lewis acid sites (the ω_{19b} vibrational mode) cannot be distinguished from the IR band of pyridine interacting via H-bonding with silanol group in silanol nests (1445 cm^{-1}).[47] The absence of bands at 1545 or 1637 cm^{-1}, indicates the absence of Brønsted acid sites strong enough to protonate pyridine.[3] Therefore, the IR band at 1490 cm^{-1} is predominantly attributed to pyridine adsorbed on La Lewis acid sites. Since the integrated intensity of the band at 1490 cm^{-1} increases linearly with increasing La/Al ratio up to 0.24 (Figure S4A), it is reasonable to conclude that La sites on La-DeAlBEA for La/Al < 0.24 are present as isolated sites. Consistent with this interpretation, the areas of IR bands for pyridine adsorption on Lewis acid sites, obtained by deconvolution from the overlapping peaks at 1560~1600 cm^{-1}, also exhibits a nearly linear dependence on the La/Al ratio up to a value of 0.24 (Figure S4B).

IR spectroscopy of adsorbed perdeuterated acetonitrile (CD_3CN) was further applied to distinguish Lewis acid sites from silanol groups.[48] IR spectra of CD_3CN

adsorbed on DeAlBEA and 0.06La-DeAlBEA taken as a function of He purging time are illustrated as Figure S5. DeAlBEA exhibits a peak at 2273 cm^{-1} characteristic of the $\nu(C \equiv N)$ stretching vibration of CD_3CN interreacting with H-bonded silanol groups (silanol nests).[48-50] For 0.06La-DeAlBEA, the center of the IR band shifts to 2287 cm^{-1} attributable to CD_3CN adsorbed on Lewis acidic sites accompanied by a shoulder peak at 2273 cm^{-1} for CD_3CN adsorption on residual silanol nests. [39, 51, 52] With increasing purge time, the peak intensity decreases due to a gradual decrease in CD_3CN coverage, but finally remains nearly constant after purging for 40 min. Quantitative analysis of Lewis acid sites was, therefore, based on the IR spectrum recorded at 50 min. Figure 2C presents IR spectra acquired for CD_3CN adsorbed on DeAlBEA and La-DeAlBEA with La/Al ratios ranging from 0.06 to 0.60. For better quantification of the integrated area of the band at 2287 cm^{-1}, peak deconvolution utilizing a fixed band center and fwhm was used to exclude the contribution from the overlapping band at 2273 cm^{-1} due to CD_3CN adsorbed on silanol nests. The area of the IR band for Lewis acid La sites shows a increases linearly up to a La/Al = 0.24 and then increases at a much lower rate for higher values of La/Al (Figure 2D). This suggests that isolated La Lewis acid sites predominate for catalysts with La/Al < 0.24, while lanthanum oxide clusters may be generated at higher La loadings.

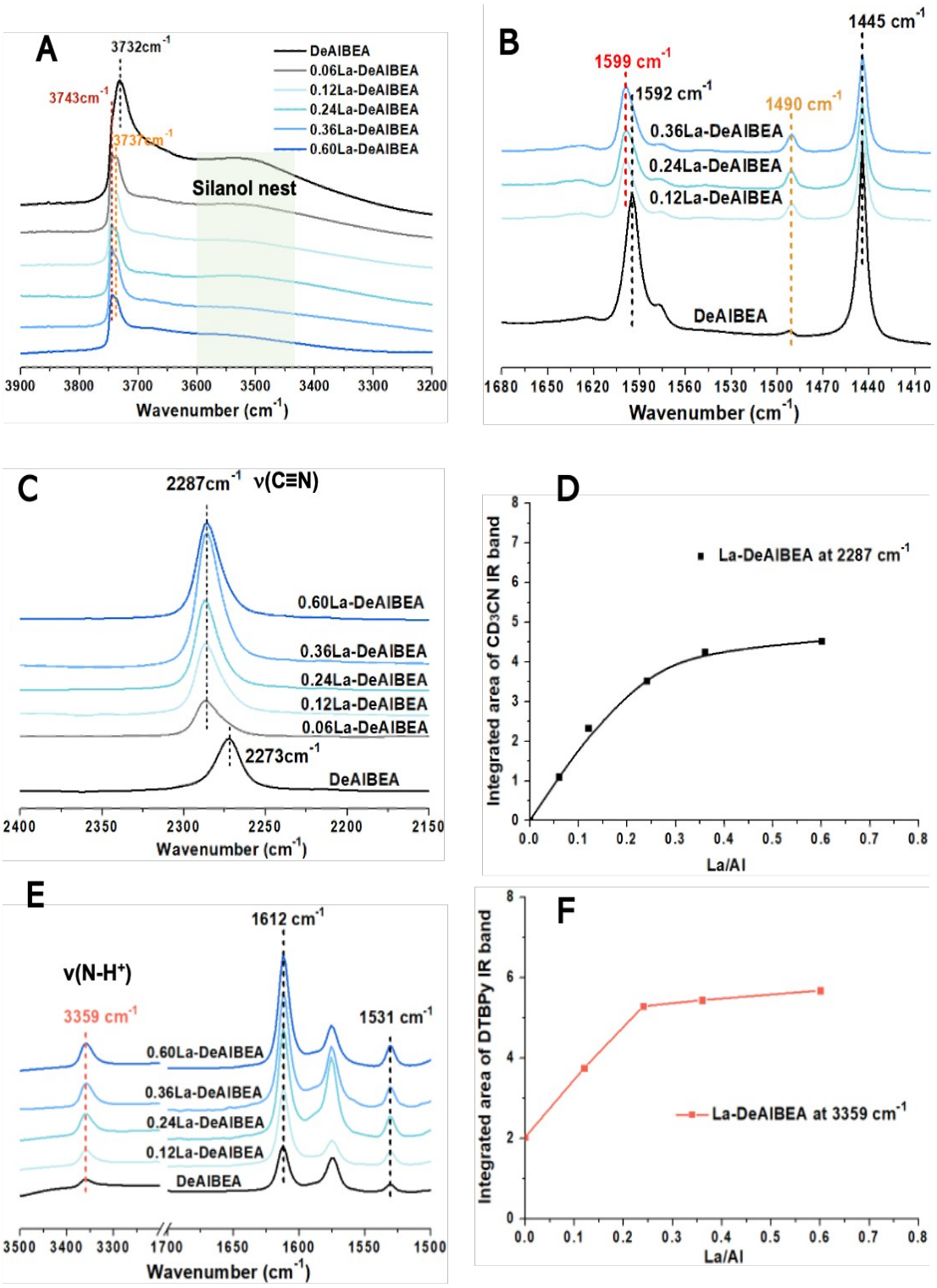

Figure 2. (A) Effect of La loadings on the FTIR spectra of the surface hydroxyl groups on DeAlBEA and La-DeAlBEA. FTIR spectra of adsorbed (B) pyridine, (C) CD_3CN and (E) DTBPy for DeAlBEA and La-DeAlBEA. Plots of the integrated area for (D) the CD_3CN adsorption band at 2287 cm^{-1} and (F) the DTBPy adsorption band at 3359 cm^{-1} versus La/Al ratio for La-DeAlBEA.

2,6-Di-*tert*-butylpyridine (DTBPy) is able to distinguish weak Brønsted acidity arising from H-bonding interaction among M-OH groups of open Lewis acid sites and adjacent silanol groups from siliceous zeolitic supports (i.e. M-OH···O(H)-Si).[7, 48, 53, 54] Previous studies have shown that all Brønsted acid sites in BEA zeolite can be accessed by DTBPy.[39, 55] Figure 2E presents the IR spectra of DTBPy adsorbed on La-DeAlBEA. Bands at 3359, 1612, and 1531 cm^{-1} for vibrations of protonated DTBPy[55] are clearly observed for all samples of La-DeAlBEA and their intensity increases with the increasing La loadings. The observed changes are attributable to DTBPy adsorption on H-bonded La-OH and Si-OH groups. The band at 3359 cm^{-1} for ν(N-H^+) vibrations is used to quantify the content of weak Brønsted acid sites.[56] As seen in Figure 2F, the integrated intensity increases linearly as the La/Al ratio increases to 0.24, suggesting that isolated La sites with La-OH group (most likely presented as open chemical structure, i.e., La sites are grafted onto two Si-O-La bonds and one hydroxyl (-OH) group) are mainly formed via grafting onto the zeolitic framework.

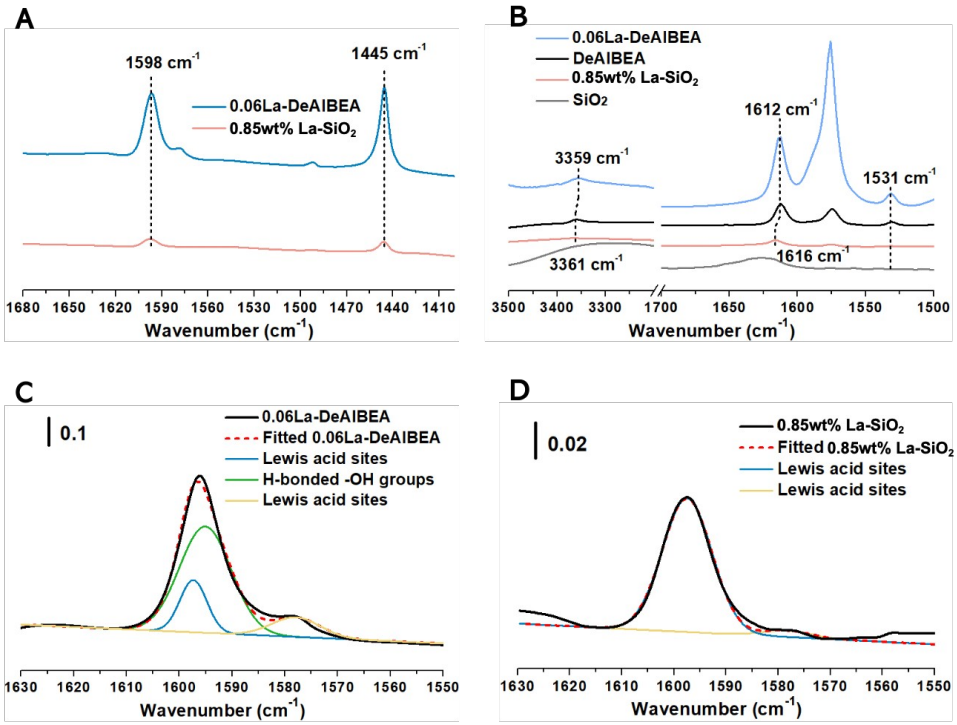

Figure 3. (A) The FTIR spectra with pyridine adsorption for 0.06La-DeAlBEA and 0.85wt%La-SiO_2. (B) FTIR spectra of adsorbed DTBPy for SiO_2, 0.85wt%La-SiO_2,

DeAlBEA and 0.06La-DeAlBEA. Deconvolution of pyridine-adsorbed FTIR spectra for (C) 0.06La-DeAlBEA and (D) 0.85wt%La-SiO_2.

The acid properties of La sites grafted onto SiO_2 (0.85wt%La-SiO_2) and DeAlBEA (0.06La-DeAlBEA) supports which have nearly identical La loadings were comparatively investigated. Figure S6 presents the IR spectra of pyridine adsorbed on 0.06La-DeAlBEA and 0.85wt%La-SiO_2 recorded after purging 5 to 25 min. Introduction of pyridine leads to the appearance of Lewis acid IR bands at around 1598 and 1445 cm^{-1} over both catalysts. We note further that the intensity of IR spectra remains almost unchanged after purging for 25 min. The IR spectra for pyridine adsorbed on 0.06La-DeAlBEA and 0.85wt%La-SiO_2 recorded at 25 min are compared in Figure 3A. As shown, the intensity of the IR bands for pyridine adsorption on 0.85wt%La-SiO_2 is much weaker than that for pyridine adsorption on 0.06La-DeAlBEA. As discussed above, the IR bands at about 1598 and 1445 cm^{-1} for 0.06La-DeAlBEA contain contributions from pyridine interacting with both La Lewis acid sites and residual H-bonded silanol nests. To distinguish the contribution of Lewis acid La sites over each catalyst, the IR band centered 1598 cm^{-1} was deconvoluted (Figures 3C, D). The integrated intensity of the band for pyridine adsorption on La Lewis acid sites on 0.06La-DeAlBEA and 0.85wt%La-SiO_2 is nearly identical (1.1 vs 0.9), suggesting the similarly high dispersion of La Lewis acid sites on both DeAlBEA and SiO_2. To further clarify the local environment of La Lewis acid sites over both supports, IR spectroscopy of adsorbed DTBPy was also employed (Figure 3B). In sharp contrast to what is observed on 0.06La-DeAlBEA, the IR bands for protonated DTBPy are nearly undetectable over SiO_2 and 0.85wt%La-SiO_2. The significantly weaker IR bands observed for 0.85wt%La-SiO_2 compared to 0.06La-DeAlBEA indicate the absence of H-bonding interaction between La-OH and Si-OH groups over SiO_2.

^{1}H MAS NMR spectroscopy was used to further characterize the changes of hydroxyl groups over DeAlBEA and La supported DeAlBEA with La/Al ratio of 0.12 and 0.24. Before analysis, spectral peak deconvolution was conducted to distinguish the overlapping peaks. As shown in Figure S7, after deconvolution, six similar peaks

can be identified for all the three samples and the estimated concentration of each -OH group was summarized in Table S1. The ^{1}H MAS NMR of DeAlBEA shows signals at 1.0, 1.7, 2.0, 2.3, 3.1 and 4.5 ppm. The peak at 1.7 ppm and the very small peak at 1.0 ppm are assigned to isolated silanol groups.[57] The peaks at 2.0 and 2.3 ppm are internal silanol groups, while the peak at 3.1 ppm represents H-bonded silanol nests.[34] The broad peak centered at larger chemical shift (4.5 ppm) is due to strongly H-bonded Si-OH groups and/or probably clusters of adsorbed H_2O.[34, 44] Introduction of La led to an obvious loss of silanol nests and internal silanols at around 3.1, 2.0 and 2.3 ppm while the peak attributable to isolated Si-OH groups remains almost unchanged (0.37~0.45 mmol/g), which clearly indicates that La species were grafted onto the silanol nests and internal silanols as found by IR characterization. ^{1}H NMR signal for La-OH groups has been reported to be characterized by a proton chemical shift of around 2.5 ppm in the super cages of X and Y zeolite,[58] which is quite close to the H-bonded internal Si-OH groups detected at 2.3 ppm. Consequently, the chemical shift at 2.3 ppm for 0.12La-DeAlBEA and 0.24La-DeAlBEA could have contributions from both La-OH groups and residual internal Si-OH groups.

IR analysis of adsorbed pyridine, CD_3CN and DTBPy on La-DeAlBEA as well as the ^{1}H MAS NMR spectroscopy reveal the generation of isolated Lewis acid sites arising from La grafting into the silanol nest on DeAlBEA and formation of weak Brønsted acid sites due to H-bonded La-OH···O(H)-Si structures. In sharp contrast, La sites grafted onto SiO_2 are predominantly present as isolated La sites with a similar open structure as that for La-DeAlBEA but no H-bonding interaction with proximal Si-OH groups.

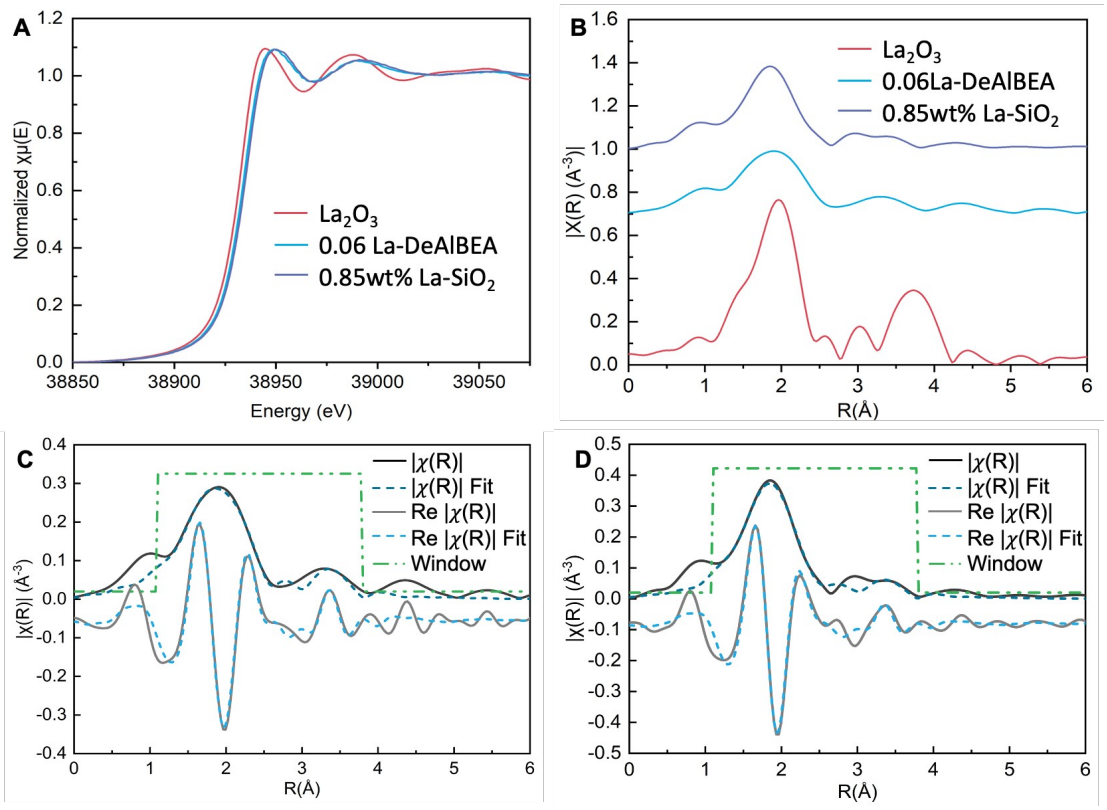

Figure 4. (A) Normalized La K-edge X-ray absorption near-edge spectra (XANES) of 0.06La-DeAlBEA and 0.85wt% La-SiO_2 catalysts as well as La standard at ambient conditions. (B) Fourier-transformed k^2-weighted extended X-ray absorption fine structure spectra (EXAFS) of 0.06La-DeAlBEA and 0.85wt% La-SiO_2 catalysts. Curve fitting of the real and imaginary components of the EXAFS data for (C) 0.06La-DeAlBEA and (D) 0.85wt%La-SiO_2 catalysts. Catalysts were pretreated at 573 K in He for 30 min.

The oxidation state and coordination geometry of La sites were investigated using X-ray absorption spectroscopy (XAS). XANES spectra for La_2O_3, 0.85wt% La-SiO_2 and 0.06La-DeAlBEA are presented in Figure 4A. The XANES spectrum of 0.06La-DeAlBEA is similar to that La_2O_3, indicating that La in La-DeAlBEA sample is best described as La(III). The EXAFS spectra of La_2O_3, 0.85wt% La-SiO_2 and 0.06La-DeAlBEA are displayed in Figure 4B. Fitting of the real and imaginary components of the Fourier transform of the EXAFS data yields the coordination number and bond distance given in Table 1. The multielectron excitations (MEE) removal process of all spectra was applied to eliminate the influence of strong multielectron excitations of La. The changes of k-space and R-space data before and

after MEE removal are shown in Figures S8 and S9. Compared to the spectrum of La_2O_3, only one strong peak was observed in the spectra of 0.85wt% La-SiO_2 and 0.06La-DeAlBEA. The absence of La-La[59] and La-O-La[60] backscattering in the second shell of the spectra of 0.06La-DeAlBEA and 0.85wt% La-SiO_2 indicates that the La atoms are isolated. The results of fitting shown in Figure 4C suggest that there are two La-O scattering paths with distance of about 2.44 Å and 2.62 Å. The first peak is attributed to the La-O bond formed upon condensation of La with two silanol groups and one La-OH group has a CN_{La-O} ~ 3, and the second peak is attributed to one dative bond with silanol group in DeAlBEA and interaction with three molecules of H_2O with a total CN_{La-O} of ~ 4.[61- 63] The two coordination distances are consistent with La containing compounds; for example, the La-O bond in La_2O_3 is in range of 2.41 - 2.50 Å [64], while the La-O bond distance in the aqueous $La(H_2O)_9^{3+}$ is ca. 2.60 Å [65]. The two bond lengths found in the best curve fitting results, together with the DTBPy-adsorbed IR results also indicate the presence of La-OH group. Hence, La is proposed to be present as $\equiv Si{-}O{-}La(OH){-}O{-}Si \equiv$ with the La also datively coordinated with one $\equiv Si{-}OH$ group and two water molecules. XAS analysis of 0.85wt%La-SiO_2 was also carried out and the corresponding XANES spectrum and EXAFS pattern are shown in Figures 4A and 4B, and the fitted EXAFS data are shown in Figure 3D, whereas fitted parameters are listed in Table 1. The curve fitting results for 0.85wt%La-SiO_2 suggest that there are 3 La-O bonds corresponding to La attached to two O atoms in the silica support and one La-OH group and another 3 bonds tentatively assigned to La-(OH_2).

Table 1. Fitted parameters for Fourier-transformed La K-edge EXAFS of La-DeAlBEA and La-SiO_2

Catalyst	Path	N_i	R_i (Å)	$\sigma_i^2 \times 10^{-3}$
	La-O	3	2.44 ± 0.02	6.0 ± 2.2
0.06La-DeAlBEA	La-O	4	2.62 ± 0.02	6.0 ± 2.2
	La-(O)-Si	3	4.01 ± 0.03	9.7 ± 5.3
0.85wt% La-SiO_2	La-O	3	2.43 ± 0.02	2.8 ± 1.2

La-O	3	2.60 ± 0.02	2.8 ± 1.2
La-(O)-Si	2	4.00 ± 0.05	9.3 ± 4.6

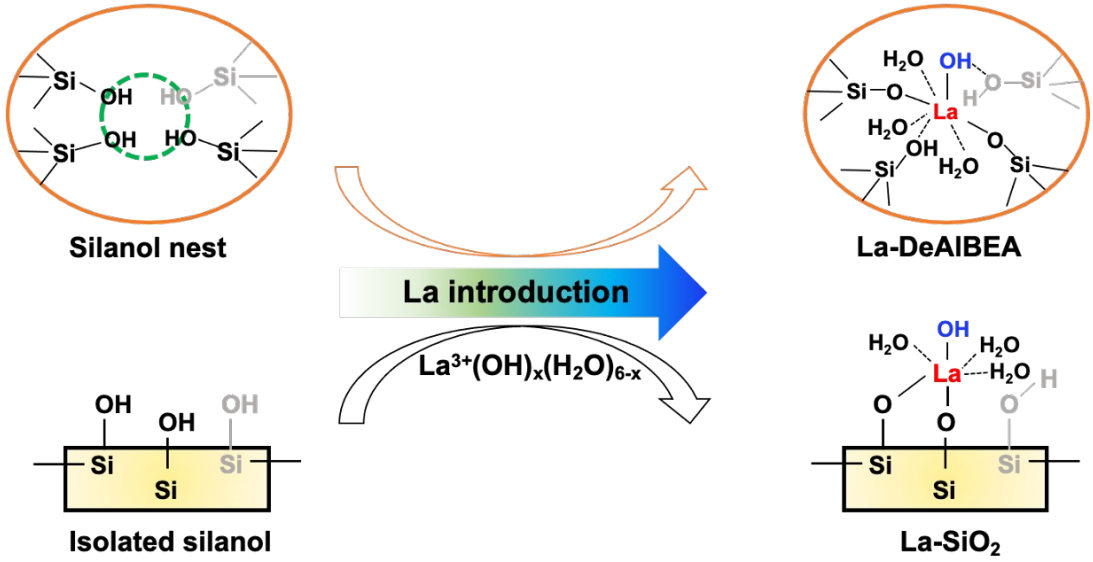

Scheme 1. Construction of La isolated sites over dealuminated Beta zeolite and SiO_2.

In summary, based on the information obtained from IR spectroscopy as well as XAS analysis of La-DeAlBEA and La-SiO_2, it is possible to propose the chemical structure of isolated La sites supported on DeAlBEA and SiO_2. As shown in Scheme 1, La in La-DeAlBEA is predominantly bonded to two O atoms of the support, one -OH group and datively coordinated with one adjacent Si-OH groups. The weak Brønsted acidity of La-DeAlBEA detected by DTBPy IR spectroscopy and the existence of strongly H-bonded silanol nests over DeAlBEA support the proposal that La-OH exhibits H-bonding interaction with Si-OH groups on DeAlBEA. In contrast to DeAlBEA, SiO_2 mainly possess isolated silanol groups[34] and no Brønsted acidity is evidenced by DTBPy IR spectroscopy for La-SiO_2. Consequently, H-bonding interactions between La sites and Si-OH groups do not appear for La supported on SiO_2.

Ethanol conversion over DeAlBEA and La-DeAlBEA

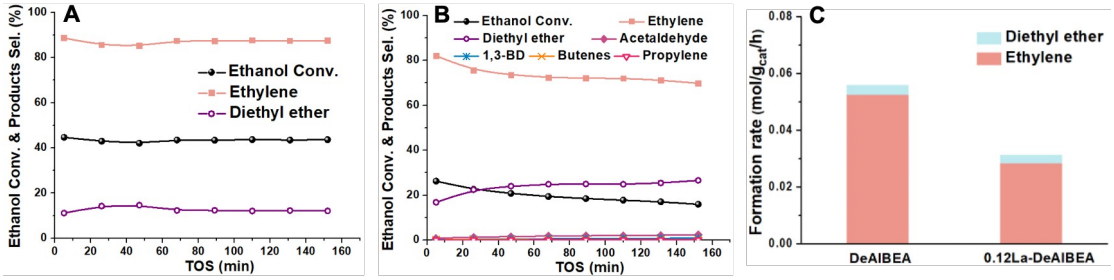

Figure 5. EtOH conversion and product distribution catalyzed by (A) DeAlBEA and (B) 0.12La-DeAlBEA as a function of time-on-stream (TOS). (C) Comparison of the initial rate of EtOH dehydration over DeAlBEA and 0.12La-DeAlBEA. Reaction conditions: m_{cat} = 20 mg, T = 603 K, F_{He} = 20 mL/min, p_{EtOH} = 5.34 kPa.

The conversion of EtOH at 603 K over DeAlBEA and La-DeAlBEA are shown in Figure 5 as a function of time-on-stream (TOS). The principal process occurring over DeAlBEA is dehydration of EtOH to produce ethene and diethyl ether (DEE), which occurs with a total selectivity of about 99.7%.[3, 21] For 0.12La-DeAlBEA, ethene and DEE remain the principal products together with a small amount of acetaldehyde (AcH) (< 2%). This suggests that Lewis acid La sites are nearly inactive for EtOH dehydrogenation.[3, 21] Note that the initial rate of EtOH dehydration over DeAlBEA is higher than that over 0.12La-DeAlBEA (Figure 5C), a consequence of the stronger acidity of silanol nests than Lewis acid La sites for catalyzing EtOH dehydration. It is also observed that the EtOH conversion over DeAlBEA remains relatively stable for 150 min, whereas that over 0.12La-DeAlBEA decreases monotonically with TOS due to gradual poisoning of the sites active for dehydration by the AcH produced, as was observed for Y-DeAlBEA.[3, 66] Li and Dai et al. have investigated the mechanism of catalyst deactivation during ethanol conversion to 1,3-BD.[66] They found that acetaldol formed by AcH aldol condensation can proceed via dehydrogenation to produce 3-

oxobutanal, which then reacts with water to produce acetone. Through a cascade self- and cross-condensation of acetaldehyde and acetone, long-chain unsaturated aldehydes/ketones are formed that further convert to 2,4-dimethyl benzaldehyde via cyclization. These processes gradually lead to coverage of the active sites and catalyst deactivation.

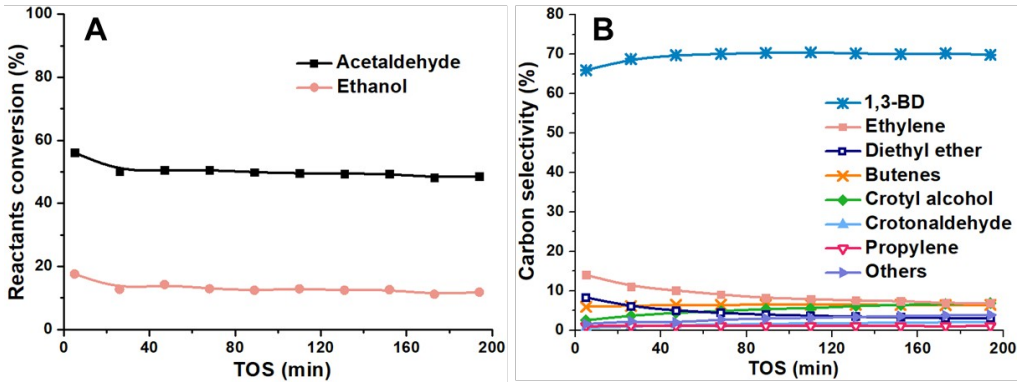

Figure 6. (A) Conversions of EtOH and AcH and (B) product distribution for EtOH-AcH conversion over 0.12La-DeAlBEA as a function of TOS. Reaction conditions: m_{cat} = 10 mg, T=603 K, $F_{EtOH\text{-}AcH}$ = 0.189 mL/h, m_{EtOH}/ m_{AcH} = 6, P_{EtOH} = 2.73 kPa, P_{AcH} = 0.48 kPa, total flow rate = 41.2 mL/min.

As can be seen in Figure 5B, almost no 1,3-BD is generated during the reaction of pure EtOH over 0.12La-DeAlBEA, suggesting that AcH is a necessary precursor for C-C bond formation in the ETB process. This reaction was investigate by feeding 0.48 kPa of AcH together with EtOH (2.73kPa), Figure 6 shows the conversion of an EtOH-AcH mixture (A) and the distribution of products formed (B) at 603 K. 1,3-BD is observed immediately after TOS = 5 min with a high initial selectivity of ~66.0% at an EtOH conversions of 17.8% and an AcH conversion of 56.2%, indicating that isolated La sites are catalytically active for C-C coupling process.[3] Moreover, as the reaction proceeds, the selectivity to 1,3-BD increases to 68.8% within the initial 20 min and then reaches a plateau of about 70% for longer TOS; concurrently, the selectivity to ethene decreases monotonically. As noted earlier, this trend is attributed to inhibition of EtOH dehydration caused by gradual AcH poisoning of the remaining

silanol nests. Figure 6B shows that other C_4 products are also observed in small proportions, most notably butenes, crotyl alcohol and crotonaldehyde, with a total selectivity below 15%.[3, 10, 15, 17, 21]

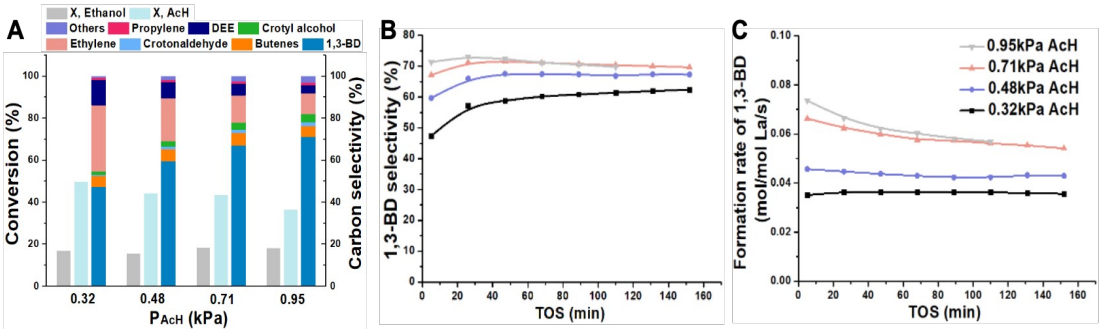

Figure 7. (A) Effect of AcH partial pressure on the conversions of EtOH-AcH mixture, and products distribution at TOS=5min. (B) The selectivity of 1,3-BD and (C) the rate of 1,3-BD formation over 0.12La-DeAlBEA as functions of AcH partial pressure and TOS. Reaction conditions: m_{cat} = 10 mg, 623 K, P_{EtOH} = 2.73 kPa, P_{AcH} = 0.32, 0.48, 0.71 and 0.95 kPa, total flow rate = 41.2 mL/min.

The reaction of EtOH and AcH was further investigated as a function of feed AcH partial pressure for a constant feed EtOH partial pressure of 2.73 kPa, as shown in Figure 7. The conversion of EtOH within the range of AcH partial pressures explored changes from 15.6% at high AcH partial pressure to 17.0% at low AcH partial pressure. As the AcH partial pressure increases from 0.32 kPa to 0.95 kPa, the selectivity towards dehydration products, mainly ethene, decreases significantly and the initial selectivity to 1,3-BD increases from 47.4% to 71.3%. Moreover, as shown in Figure 7B, the induction period for obtaining a stable 1,3-BD selectivity shortens remarkably at higher AcH partial pressures. Figure 7C illustrates the rate of 1,3-BD formation as functions of AcH partial pressure and TOS. The introduction of AcH enhances the formation of 1,3-BD significantly. All these observations point to AcH inhibition of EtOH dehydration and promotion of C-C coupling. However, we note that if the AcH partial pressure is too high, the catalyst stability is impaired due to enhanced formation of oxygen or non-oxygen containing coke precursors.[14, 66] This result supports the hypothesis that deactivation occurs via a combination of self- and cross-condensation of AcH and acetone that produces long-chain unsaturated aldehydes/ketones which lead to coverage of the active sites and their deactivation. It

is noted, though, that the catalyst could be regenerated by calcination in air atmosphere at high temperature of 823 K.[66]

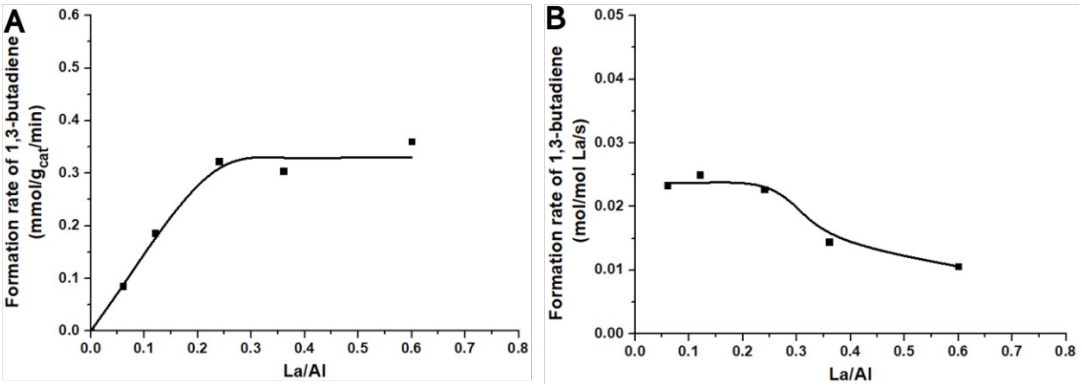

Figure 8. Initial formation rates of 1,3-BD from EtOH- AcH conversion, measured at 2.73 kPa EtOH and 0.32 kPa AcH and 573 K, as a function of La/Al ratio. (A) Rates normalized per catalyst mass. (B) Rates normalized per moles of La. The turnover of frequency (TOF) rates of 1,3-BD formation for La-DeAlBEA with varying La contents are tested based on identical space velocity relative to La amount.

To clarify the effect of the nature of La species on their activity for C-C coupling, initial rates of 1,3-BD formation at TOS = 5 min were measured at 573 K under differential reaction conditions using a feed containing 2.73 kPa EtOH and 0.32 kPa AcH as a function of La/Al ratio. As observed in Figure 8A, the rate of 1,3-BD formation normalized per gram of catalyst increases linearly with La loading up to a La/Al ratio of 0.24, but then reaches a plateau for higher values. When the rate of 1,3-BD formation is normalized per atom of La (Figure 8B), the rate is nearly independent of the La/Al ratio for values of 0.06 to 0.24, suggesting that the active La sites are isolated. Previous studies support this conclusion, suggesting that isolated Lewis acid Ta[38], Zr,[4] and Y[3, 32] sites are the active centers for C-C bond formation. As the La/Al ratio increases from 0.24 to 0.60, the TOF rate of 1,3-BD formation decreases continuously, which may indicate the generation of less active LaO_x clusters or nanoparticles at higher La loadings. These experimental results agree well with the IR and XAS characterization results reported in Figures 2 and 4.

The specific roles of isolated La Lewis acid sites in the critical steps of the ETB process were explored further by decoupling the reaction network. The first step investigated was aldol condensation of AcH to crotonaldehyde, since this reaction is generally regarded as critical for the formation of C-C bonds in the ETB process, and it has been suggested that this step is catalyzed by isolated Lewis acid site.[15, 17, 18, 67] However, investigation of the mechanism by which isolated Lewis acid catalyzed AcH aldol condensation is still encumbered by rapid site deactivation,[15] which makes investigation of the kinetics and mechanism challenging.

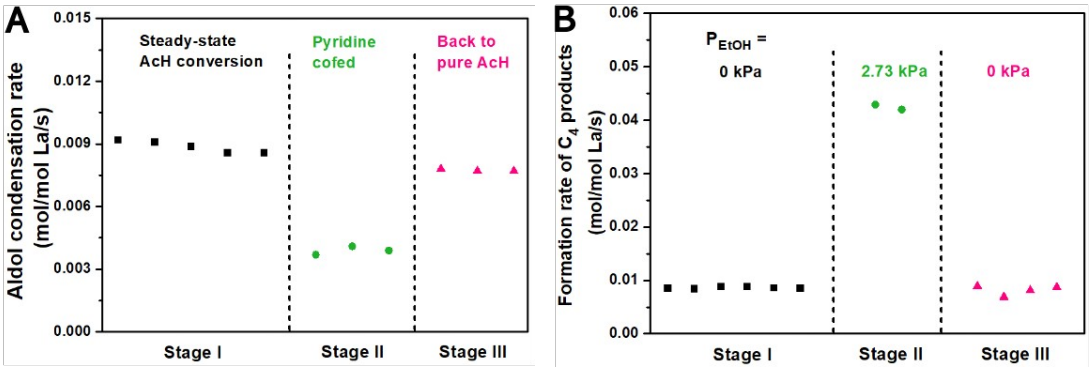

Figure 9. (A) Transient formation rates of crotonaldehyde from AcH conversion over 0.06La-DeAlBEA during introduction and removal of pyridine. Without EtOH, crotonaldehyde is produced with selectivity above 95%. After introducing EtOH, 1,3-BD is formed with selectivity of about 65%. (B) Transient formation rates of C_4 products over 0.06La-DeAlBEA during introduction and removal of EtOH. Reaction conditions: 573 K, m_{cat} = 10 mg, p_{AcH} = 0.41 kPa, total flow rate = 40.5 mL/min.

As shown in Figure 9, pure AcH forms crotonaldehyde with a selectivity close to 100% and at a stable rate of about 0.009 mol/mol La/s over 0.06La-DeAlBEA under the reaction conditions chosen. Notably, acetaldol is not observed, indicating that the dehydration of acetaldol to produce crotonaldehyde is rapid. To elucidate the site requirements for AcH aldol condensation, pyridine was introduced continuously with the feed to titrate Lewis acid La sites. The rate of crotonaldehyde formation decreases rapidly from 0.009 to 0.004 mol/mol La/s upon introduction of 0.12 kPa of pyridine, but immediately returns back to 85% of the original rate when the flow of pyridine is

terminated. This suggests that La Lewis acidic sites play a catalytic role in AcH aldol condensation.

In our earlier work on Y-DeAlBEA, it was proposed that addition of EtOH to AcH resulted in 1,3-BD formation via concerted EtOH-AcH coupling.[3] To assess whether this pathway was also operative for La-containing catalysts, we compared feeding pure AcH and EtOH-AcH over 0.06La-DeAlBEA. Pure AcH was fed into the reactor first and then the feed was switched to an EtOH-AcH mixture while maintaining the same AcH partial pressure, and finally the feed was switched back to pure AcH. As shown in Figure 9B, with pure AcH as the feed, crotonaldehyde forms at a stable rate of ~0.009 mol/mol La/s. When 2.73 kPa of EtOH is introduced into the AcH feed stream, the rate of C_4 products (principally 1,3-BD) increases by a factor of 4.8 to 0.043 mol/mol La/s. The C_4 product formation rate drops back to ~ 0.009 mol/mol La/s when the flow EtOH is stopped. The reactant switching experiments clearly demonstrate the participation of EtOH in the generation of new C-C bonds, like what we observed over Y-DeAlBEA.[3] Additionally, the rate of C_4 products formation over La-DeAlBEA is determined to be 0.035 mol/mol La/s with 2.7 kPa ethanol and 0.3 kPa AcH at 573 K based on the kinetics discussed below. This activity is slightly higher than that for Y-DeAlBEA under identical reaction conditions (0.0287 mol/mol Y/s).

It is notable that the conversion of AcH over 0.06La-DeAlBEA and 0.85%La-SiO_2 for identical rection conditions gives near-identical rates of crotonaldehyde formation (Figure S10), suggesting that La Lewis acid sites on 0.06La-DeAlBEA and 0.85%La-SiO_2 are responsible for aldol condensation of AcH, despite the differences in extent of local H-bonding local environment. As analyzed by pyridine adsorbed IR spectroscopy, the amounts of Lewis acid La sites over 0.06La-DeAlBEA and 0.85%La are nearly identical. However, in the case of EtOH-AcH conversion, no significant enhancement in the C-C formation rate was observed compared with pure AcH conversion over 0.85wt%La-SiO_2, suggesting that the Lewis acid center local environment, H-bonding interaction of La-OH with Si-OH groups of zeolite

framework, participates in the C-C bond formation under EtOH co-feeding conditions.

According to the traditional reaction mechanism for the ETB process, two molecules of AcH react to produce crotonaldehyde, which then react with EtOH to produce crotyl alcohol and AcH via the MPV reaction.[4, 14] The resulting crotyl alcohol then rapidly dehydrates to form 1,3-BD.[7] To gain additional insights into the active sites responsible for each reaction step and to identify the rate-limiting step in the overall reaction, we investigated the reaction of AcH-EtOH, crotonaldehyde-EtOH, and crotyl alcohol over DeAlBEA and 0.06La-DeAlBEA, respectively. The rates of product formation in these studies are summarized in Table 2. Cofeeding 0.16 kPa crotonaldehyde and 2.73 kPa EtOH at 573 K over 0.06La-DeAlBEA produces 1,3-BD at the rate of 0.143 mmol/g_{cat}/min and total C_4 products (butenes and crotyl alcohol) at the rate of 0.155 mmol/g_{cat}/min. These observations demonstrate almost complete conversion of crotonaldehyde, indicating that the MPV reaction between crotonaldehyde and EtOH proceeds rapidly for this catalyst under the reaction conditions investigated. By contrast, under similar conditions, only a negligible amount of 1,3-BD is produced over DeAlBEA. This observation suggests that the La Lewis acid sites are required to catalyze the MPV reaction, in line with the previous reports of Zn, Y and La-containing catalysts.[14, 20]

When 0.16 kPa or 0.32 kPa crotyl alcohol was fed to the reactor containing 0.06La-DeAlBEA, 1,3-BD was produced at the rate of 0.096 and 0.155 mmol/ g_{cat}/min, respectively, suggesting that crotyl alcohol preferentially undergoes intramolecular dehydration and this is a facile step in the process. Importantly, it is also noted that the rates of C_4 products formation via MPV and crotyl alcohol dehydration are both higher than that observed when AcH and EtOH are fed at a similar carbon-based flowrate (0.087 mmol/g_{cat}/min), indicating that C-C bond formation process is the rate-limiting step for AcH-EtOH conversion to 1,3-BD over La-DeAlBEA.

Table 2. Conversion of intermediates over DeAlBEA and 0.06La-DeAlBEA

catalyst	reactants	formation rate, mmol/g_{cat}/min			
		1,3-BD	butenes	crotyl alcohol	C_4 products
0.06La-DeAlBEA	AcH-EtOH[a]	0.087	0.005	0.004	0.096
	crotonaldehyde-EtOH[b]	0.143	0.006	0.006	0.155
	crotyl alcohol[c]	0.096	0.002	--	0.098
	crotyl alcohol[d]	0.155	0.003	--	0.158
DeAlBEA	crotonaldehyde-EtOH[b]	0.015	--	--	0.015
	crotyl alcohol[c]	0.121	0.002	--	0.123

Reaction conditions: T= 573 K, m_{cat} = 0.02 g, He flow rate = 40 mL/min; [a]AcH and EtOH (EtOH) reaction was measured with 0.32 kPa AcH and 2.73 kPa EtOH; [b]Conversion of crotonaldehyde and EtOH was measured with 0.16 kPa crotonaldehyde and 2.73 kPa EtOH; Conversion of crotyl alcohol was measured with crotyl alcohol partial pressures of [c]0.16 kPa and [d]0.32 kPa, respectively.

As discussed before, both the MPV reaction and crotyl alcohol dehydration are facile over La-DeAlBEA and C-C bond formation is the rate-limiting step. Therefore, the rate enhancement observed upon cofeeding EtOH and AcH suggests that EtOH reacts directly with AcH to form a C-C bond during 1,3-BD synthesis over La-DeAlBEA, as was proposed for the occurrence of this reaction over isolated Y sites in Y-DeAlBEA.[3]

The experiments involving the conversion of reaction intermediates and switching of reactants, suggest that the grafted $(\equiv SiO)_2La{-}OH{\cdots}HO{-}Si\equiv$ groups present in La-DeAlBEA are responsible for catalyzing AcH aldol condensation, the MPV reaction and crotyl alcohol dehydration. Moreover, the silanol nests in DeAlBEA can also promote the crotyl alcohol dehydration. When EtOH is cofed with AcH, C_4 product formation is enhanced by 4.8-fold, which is attributed to the opening up of a new C-C formation pathway involving EtOH and AcH. Comparison of EtOH-AcH conversion over 0.06La-DeAlBEA and 0.85wt%La-SiO_2, the new C-C bond formation route is found to be closely related to the H-bonding interaction between La-OH sites and silanol groups presented in DeAlBEA ($(\equiv SiO)_2La{-}OH{\cdots}HO{-}Si\equiv$). Considering the description of the chemical structure and local environment of La

sites over these two supports (DeAlBEA and SiO_2), a plausible explanation is that the Lewis acidic La center catalyzes C-C bond formation from AcH via aldol condensation, while the weak Brønsted acidity arising from the H-bonding La-OH and silanol groups $(\equiv SiO)_2La{-}OH\cdots HO{-}Si\equiv$ in La-DeAlBEA contributes to C-C bond formation between EtOH and AcH.

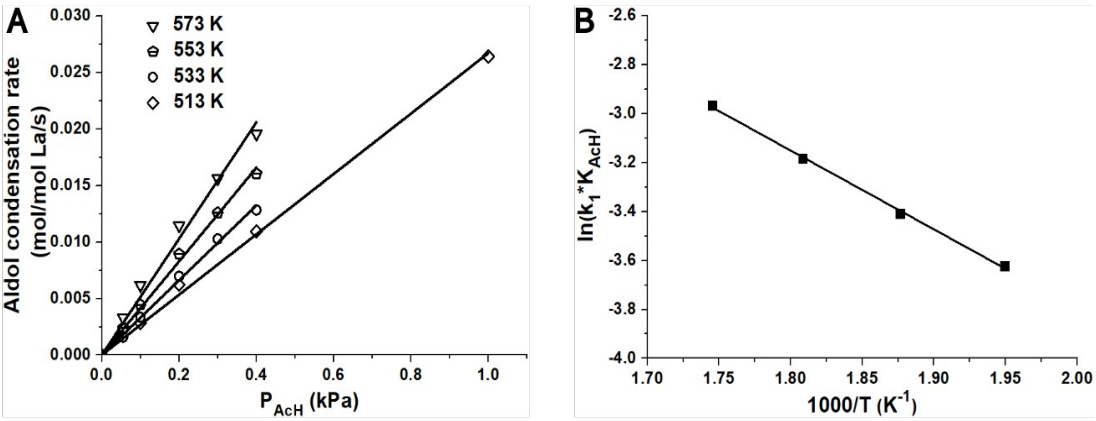

Figure 10. (A) Dependence of aldol condensation rate on the partial pressure of acetaldehyde and temperature and (B) Arrhenius plot for acetaldehyde aldol condensation over 0.06La-DeAlBEA. Reaction conditions: 513~573 K, m_{cat} = 10 mg 0.06La-DeAlBEA, total flow rate = 160 mL/min.

To further understand the two C-C formation processes, the kinetics of AcH aldol condensation and EtOH-AcH to 1,3-BD were investigated over La-DeAlBEA. The kinetics of AcH aldol condensation was explored by varying the AcH partial pressure and the reaction temperature, while maintaining a constant total flow rate. In these experiments crotonaldehyde was observed as the only product and catalyst deactivation did not exceed 10% after testing at all reaction conditions. The conversion of AcH was kept below 10% at the lowest AcH partial pressure and the highest temperature to achieve close to differential conditions. Under these conditions, the rate of crotonaldehyde formation is independent of spacetime (Figure S11A). As shown in Figure 10A, the rate of crotonaldehyde formation is first order in acetaldehyde partial pressure (< 1.0 kPa) for all reaction conditions tested. A nearly first-order dependence suggests that the adsorption of AcH over isolated La sites is

weak and that enolization of AcH is most likely the rate-limiting in the aldol condensation, in agreement with previous studies over hydroxyapatite and ZrO_2/SiO_2.[4, 10] The rate expression for AcH aldol condensation without ethanol cofeeding presented as eq. 3 below was derived with the following assumptions: the adsorption and desorption of AcH and crotonaldehyde are quasi-equilibrated; the concentration of intermediate species and AcH on the surface is negligible and the formation of AcH enolate is rate-limiting. Eq. 3 was fitted to the measured rate data shown in Figure 10A to obtain the apparent first-order rate coefficients (k_1*K_{AcH}) for AcH aldol condensation. From an Arrhenius plot of the rate coefficient (Figure 10B), the experimentally measured apparent activation energy for AcH aldol condensation is estimated to be 26.8 kJ/mol.

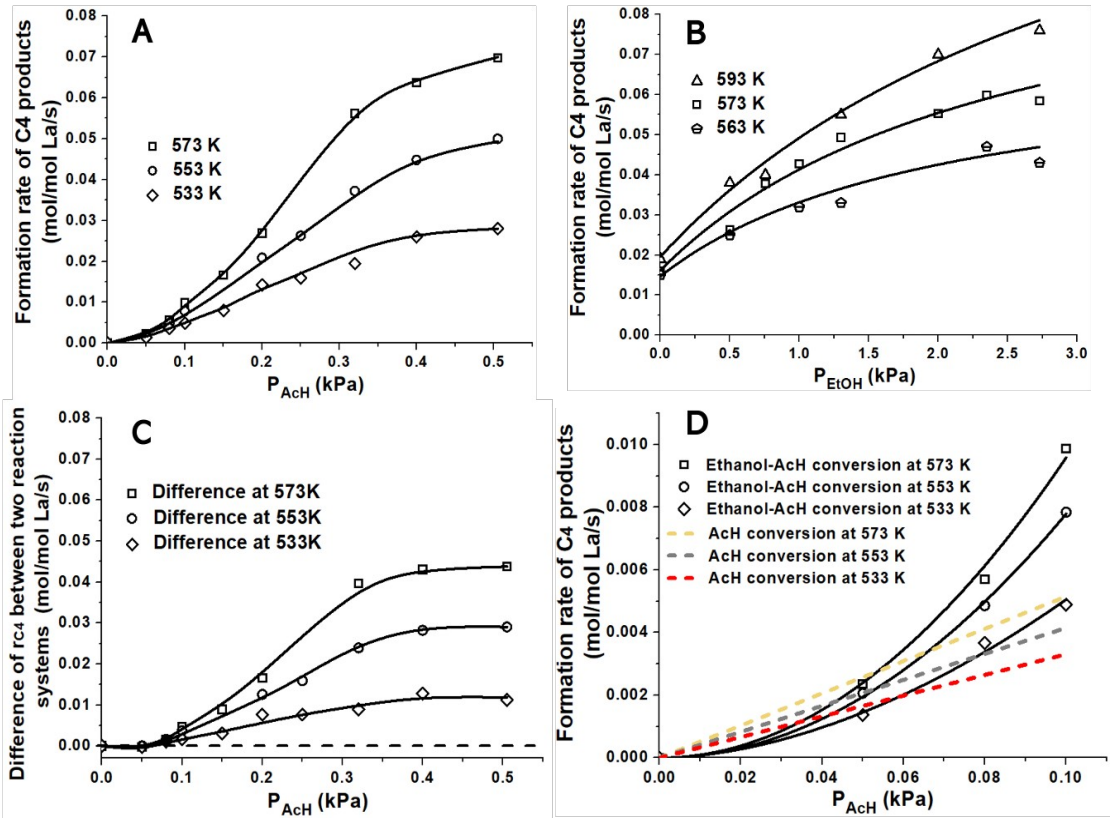

Figure 11. (A) Dependence of the rate of C_4 products formation on the AcH partial pressure, measured at 573, 553, and 533 K with 2.73 kPa EtOH. (B) Effects of EtOH partial pressure on the rate of C_4 products formation, measured at 593, 573 and 563 K with 0.32 kPa AcH. The solid lines are fittings to eq. 5. (C) Difference of the C_4 products formation rates between AcH aldol condensation and EtOH-AcH conversion

with 2.73 kPa EtOH. (D) Comparison of the C_4 products formation rates from AcH aldol condensation and EtOH-AcH conversion at AcH partial pressure below 0.1 kPa and 2.73 kPa EtOH. The solid lines in panel A, C and D are guides for eyes. Reaction conditions: 533~593 K, m_{cat} = 10 mg 0.06La-DeAlBEA, total flow rate = 80 mL/min.

The effects of the partial pressures of EtOH and AcH on the rates of C-C formation over isolated La sites on La-DeAlBEA were also explored and the results are shown in Figure 11. For investigation of the effects of AcH partial pressure, EtOH and AcH were cofed with the EtOH partial pressure held constant at 2.73 kPa, while the partial pressure of AcH was varied from 0.055 to 0.505 kPa. The conversions of EtOH and AcH were kept below 8% and 25% respectively for all reaction conditions tested. Spacetime investigation of EtOH-AcH conversion (Figure S11B, S11C) indicates that the rate of C_4 products formation is independent in the space velocity. As shown in Figure 11A, the increase in AcH partial pressure leads to a rapid increase in the formation rate of all C_4 products including 1,3-BD and small amounts of butenes and crotyl alcohol (3%-15% of the total rate of C_4 product formation) for temperatures of 533, 553, and 573 K. Notably, the rate of C_4 products formation increases remarkably for AcH partial pressures < 0.32 kPa and then increases further but at a lower rate for higher AcH partial pressures. At AcH partial pressure > 0.40 kPa, the dependence on AcH partial pressure decreases to nearly zero order as expected because AcH eventually saturates the H-bonded (≡ SiO)$_2$La–OH···HO–Si ≡ sites.

As demonstrated above, EtOH is involved directly in C-C bond formation and the rate of 1,3-BD formation via the reaction of EtOH and AcH is 4.8 times than that observed in the absence of EtOH at 573 K with 0.42 kPa AcH. The dependence of the rates of C_4 products formation on EtOH partial pressure was then investigated for a constant AcH partial pressure of 0.32 kPa at 563, 573 and 593 K. Figure 11B shows that the rates of C_4 products formation increase almost linearly with increasing EtOH partial pressure up to about 1.3 kPa and then increase but at a lower rate for higher EtOH partial pressure. Generally, the rate of C-C bond formation increases with both EtOH and AcH partial pressures, consistent with the behavior found for Y-

DeAlBEA.[3] The rate of direct coupling between AcH and EtOH is expected to be zero to positive order in AcH and EtOH partial pressure, respectively, which also agrees with the experimental results shown in Figures 11A, B.

In summary, the overall rate of C-C bond formation is due to both AcH aldol condensation and direct EtOH-AcH coupling, the contribution of each process varying with the partial pressure of EtOH and AcH. The difference of C_4 products formation rates between EtOH-AcH mixture conversion and pure AcH conversion as functions of AcH partial pressure and temperature is shown in Figure 11C. As the AcH partial pressure increases from 0.05 kPa to around 0.3 kPa, the fraction of C_4 products formed from EtOH-AcH conversion compared to AcH condensation without EtOH cofeeding increases monotonically and then reaches a plateau for higher AcH partial pressures. It is notable that the rate of C_4 products formation from EtOH-AcH conversion is slightly lower relative to the rate of AcH aldol condensation during pure AcH conversion for AcH partial pressure below 0.05kPa (Figure 11C, D). This observation is attributed to the competitive adsorption of EtOH at remarkably lower AcH partial pressures, which inhibits both the rates of AcH aldol condensation and EtOH-AcH direct coupling. With further increase in the AcH partial pressure up to 0.5 kPa, both the AcH aldol condensation and direct EtOH-AcH coupling contributes to the formation of C_4 products. While Figure 10C clearly shows that direct EtOH-AcH coupling is the main pathway for C-C bond formation at constant EtOH partial pressure of 2.73 kPa and AcH partial pressure (< 0.5 kPa). Above an AcH partial pressure of 0.5 kPa, the difference in the rate of C_4 products formation between EtOH-AcH condensation and AcH aldol condensation reaches a plateau. It is hypothesized that at higher AcH concentrations the EtOH-AcH coupling may become inhibited due to the competitive adsorption of AcH.

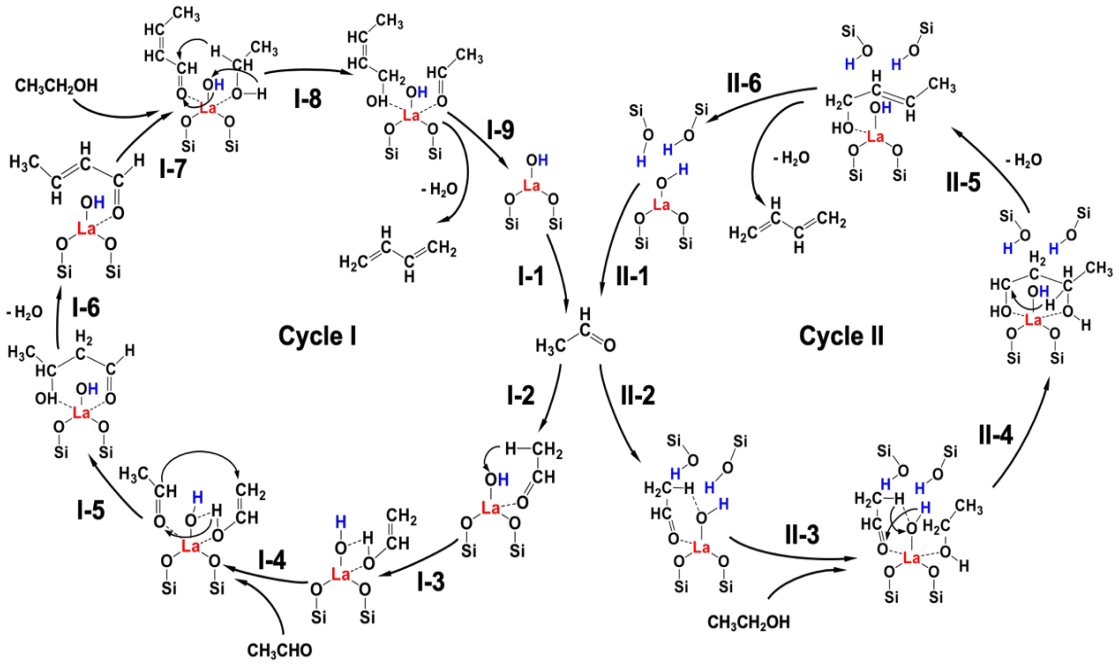

Scheme 2. Illustration of AcH and EtOH-AcH mixture conversion over isolated La sites supported on DeAlBEA.

Based on the reaction intermediates identified, the mechanism for the conversion of EtOH and AcH to 1,3-BD is envisioned to proceed as illustrated in Scheme 2. The reaction process comprises two reaction cycles. In Cycle I, 1,3-BD is formed via aldol condensation of AcH over Lewis acid La sites, whereas in Cycle II, 1,3-BD proceeds via EtOH-AcH coupling over H-bonding (≡ SiO)$_2$La–OH···HO–Si ≡ sites. Ivanova et al. have reported that aldol condensation follows a stepwise pathway involving intermediate enol formation over Lewis acid Zr catalysts.[4] Accordingly, Cycle I begins with AcH adsorption on the Lewis acid La sites and involves interaction of the nucleophilic oxygen of the carbonyl group with the electrophilic La, as depicted in Step I-1, Scheme 2.[34] Polarization of the carbonyl group in AcH is envisioned to enhance the acidity of the α-H (in the methyl group of adsorbed AcH) and therefore facilitates the α-H abstraction by the Lewis basic hydroxyl oxygen (La-OH) to form AcH enolate. Studies of butanal self-condensation over isolated Ti-OH species[68] and EtOH conversion to butadiene over Ag/ZrO$_2$/SiO$_2$[4], have reported a kinetic H/D isotope effect for both reactions, suggesting that α-H abstraction is the rate-limiting step (Step I-3) for the aldol condensation. Consistent with these findings, the kinetics

of AcH aldol condensation are first-order in AcH partial pressure, implying that enolate formation (rather than C-C coupling) is rate-limiting. Due to the absence of strong basic sites, the enolate intermediate is likely stabilized via coordination to weak basic oxygen atoms associated with La, as suggested for Zr-SiO_2 and ZrBEA.[4, 7] Subsequently, adsorption of the second AcH molecule results in the formation of a penta-coordinated species. C-C coupling of the nucleophilic carbon of the enolate intermediate with the electrophilic carbonyl carbon of the secondary adsorbed AcH forms acetaldol (Step I-5) which dehydrates rapidly to produce crotonaldehyde (Step I-6), as evidenced by the absence of acetaldol during AcH conversion. In the presence of EtOH, crotonaldehyde is envisioned to undergo rapid hydrogenation to crotyl alcohol via MPV hydrogen transfer from EtOH over La sites (Step I-7). Subsequent dehydration of crotyl alcohol (Step I-8) forms 1,3-BD (Step I-9) and another molecule of AcH. The direct coupling of EtOH-AcH (Cycle II) is envisioned to start with the stepwise adsorption of AcH and EtOH over Lewis acid La sites via an acid-base interaction (Step II-2 and Step II-3), similar to that proposed for Y-DeAlBEA.[3] After that, concerted H abstraction of adsorbed AcH by the basic oxygen atom in La-OH group and protonation of the carbonyl oxygen of AcH by the hydrogen atom of H-bonded La-OH group is thought to occur (Step II-4), resulting in the formation of AcH enolate species. The next step is the rate-limiting C-C bond formation via reaction of the α-C in EtOH with the α-C in AcH (Step II-5). This step is proposed based on exploration of the positive effects of AcH and EtOH partial pressures on the rate of 1,3-BD formation. The following step involves cleavage of α C-H group in EtOH and H transfer to the enolate intermediate, as well as dehydration to form crotyl alcohol (Step II-6). Finally, dehydration of crotyl alcohol over $(\equiv SiO)_2La{-}OH\cdots HO{-}Si\equiv$ site produces 1,3-BD, completing the reaction cycle (Step II-7).

The mechanism presented in Scheme 2 allows us to derive two rate expressions for the C_4 products formation (see SI for details). Eq. 1 is derived for the case in which the C-C bond formation is realized via AcH aldol condensation taking the

formation of enol of AcH as the rate-limiting step, and eq. 2 is derived for the case in which the C-C bond is formed by direct coupling of EtOH and AcH.[3] In both cases, the adsorption and desorption of reactants are assumed to be quasi-equilibrated and the surface coverages of intermediates are taken to be insignificant under differential reaction conditions.

$$r_{AcH-AcH}=\frac{k_1 K_{AcH} P_{AcH}}{1+K_{EtOH} P_{EtOH}+K_{AcH} P_{AcH}+K_{AA} K_{AcH}\left[P_{AcH}\right]^2+K_Y P_{EtOH} P_{AcH}} \quad (1)$$

$$r_{AcH-EtOH}=\frac{k_Y K_Y P_{EtOH} P_{AcH}}{1+K_{EtOH} P_{EtOH}+K_{AcH} P_{AcH}+K_{AA} K_{AcH}\left[P_{AcH}\right]^2+K_Y P_{EtOH} P_{AcH}} \quad (2)$$

In eq. 1, the parameter k_1 is the rate coefficient for the formation of AcH enolate, P_{AcH} and P_{EtOH} are the partial pressures of AcH and EtOH; K_{AcH} and K_{EtOH} are the equilibrium constants for AcH and EtOH adsorption onto H-bonded $(\equiv SiO)_2La{-}OH\cdots HO{-}Si\equiv$ sites; K_Y is the equilibrium constant for EtOH and AcH co-adsorption; and K_{AA} is the equilibrium constant for co-adsorption of two AcH molecules. The inhibition of adsorbed AcH and product crotonaldehyde molecules is expected to be insignificant due to the low AcH partial pressure and differential reaction conditions. For the C-C bond formation between EtOH and AcH (eq. 2), k_Y represents the rate coefficient for the direct C-C coupling of AcH and EtOH.

When pure AcH is fed, the rate of C-C coupling is the aldol condensation rate and eq. 1 simplifies to eq. 3. In the case when EtOH and AcH are co-fed, the rate of C-C coupling is the sum of the two reaction pathways and the rate expression is given by eq. 4.

$$r_{C-C\,coupling}^{A-A}=k_1 K_{AcH} P_{AcH} \quad (3)$$

$$r_{C-C\,coupling}^{A-E}=\frac{k_1 K_{AcH} P_{AcH}+k_Y K_Y P_{EtOH} P_{AcH}}{1+K_{EtOH} P_{EtOH}+K_A P_{AcH}+K_{AA} K_{AcH}\left[P_{AcH}\right]^2+K_Y P_{EtOH} P_{AcH}} \quad (4)$$

$$r_{C-C\,coupling}^{A-E}=\frac{k_1 K_{AcH} P_{AcH}+k_Y K_Y P_{EtOH} P_{AcH}}{1+K_{EtOH} P_{EtOH}+K_Y P_{EtOH} P_{AcH}} \quad (5)$$

$$r_{C-C\,coupling}^{A-E}=k_1 K_{AcH} P_{AcH}+k_Y K_Y P_{AcH} P_{EtOH} \quad (6)$$

$$r_{C-C\,coupling}^{A-E} = \frac{k_1 K_{AcH} P_{AcH}}{(K_{EtOH} + K_Y P_{AcH}) P_{EtOH}} + \frac{k_Y K_Y P_{AcH}}{K_{EtOH} + K_Y P_{AcH}} \qquad (7)$$

Eq. 3 was fitted to the measured rate data shown in Figure 9A to obtain the apparent first-order rate coefficients (k_1*K_{AcH}) for AcH aldol condensation, and the fitted results are listed in Table 3. Figure 12A shows the parity plot and the value of R^2 is 0.99, suggesting the accurate description of eq. 3 to AcH aldol condensation rates obtained experimentally. From an Arrhenius plot of the rate coefficient (Figure 10B), the experimentally measured apparent activation energy for AcH aldol condensation is about 26.8 kJ/mol. The observed effects of AcH and EtOH partial pressures on the rate of C-C coupling seen in Figure 11 are consistent with the rate laws of the form derived here for EtOH-AcH conversion system (eq. 4) proposed based on the reaction mechanisms illustrated in Scheme 2.

Since the rate of AcH aldol condensation has a first-order dependence on the AcH partial pressure, the third term ($K_A P_{AcH}$) and forth term ($K_{AA} K_{AcH} [P_{AcH}]^2$) in the denominator of eq. 4 are taken to be insignificant and, hence, eq. 4 can be simplified as eq. 5. Moreover, at constant AcH partial pressure, for low EtOH partial pressure, the second term ($K_{EtOH} P_{EtOH}$) and fifth term ($K_Y P_{EtOH} P_{AcH}$) in the denominator of eq. 5 can also be assumed to be negligible, and eq. 5 can be further simplified to eq. 6, which suggests the rate of C-C coupling is first order in the EtOH partial pressure. As the EtOH partial pressure increases to much higher values, $K_{EtOH} P_{EtOH}$ and $K_Y P_{EtOH} P_{AcH}$ are expected to be much larger than 1 and eq. 5 can thus be simplified further to eq. 7. At constant low AcH partial pressure, the second term, $\frac{k_Y K_Y P_{AcH}}{K_{EtOH} + K_Y P_{AcH}}$, is constant and the first term in eq. 7 decreases gradually as the EtOH partial pressure increases, reaching plateau at higher EtOH partial pressure. Overall, eq. 5 agrees very well with the experimental results, increasing linearly at lower EtOH partial pressure and then gradually reaching a plateau at much higher EtOH partial pressure (see Figure 11B).

Eq. 5 was fit to the measured rate data in Figure 11B by nonlinear least-squares regression. The fitted rate parameters are given in Table 4. The quality of the fit is high as can be judged by the parity plot shown in Figure 12B (the value of R^2 is 0.98). The estimated enthalpy for adsorption of EtOH (ΔH_{ads}) is −47.5 kJ/mol, and the enthalpy for co-adsorption of EtOH and acetaldehyde is −67.9 kJ/mol. The intrinsic activation energy for the concerted EtOH and AcH C-C coupling step is around 86.9 kJ/mol. The adsorption energy of AcH over isolated $(\equiv SiO)_2$-Y-OH site has been reported to be -102.3 kJ/mol, and the activation barrier for aldol condensation to be 157.3 kJ/mol over these sites.[69] Over isolated $(\equiv SiO)_2$-La-OH site, the experimentally measured apparent activation energy for AcH aldol condensation is about 26.8 kJ/mol. Considering the slightly lower Lewis acidity of La compared to Y, the adsorption enthalpy for AcH on La Lewis acid center should be lower (i.e., more positive, > 102.3 kJ/mol) than that for Y Lewis sites. On that basis, the intrinsic activation barrier for AcH aldol condensation over isolated $(\equiv SiO)_2$-La-OH site is estimated to be slightly lower than 129.1 kJ/mol. The intrinsic activation energy of EtOH and AcH C-C coupling, 86.9 kJ/mol, is most likely lower than the AcH adol condensation.

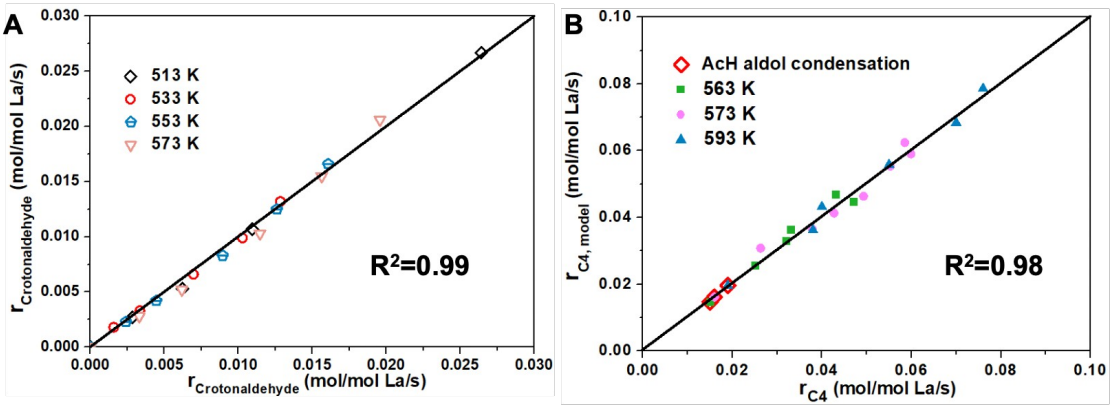

Figure 12. Parity plots for (A) the aldol condensation rate of AcH and (B) the formation rate of C_4 products from AcH-EtOH conversion obtained experimentally and fitted from eqs. 3 and 5.

Table 3. Rate parameters for C_4 products formation from AcH conversion over La-DeAlBEA

entry	First-order coefficient, mol mol La^{-1} s^{-1} kPa^{-1}				Apparent E_a, kJ/mol
Temperature, K	513	533	553	573	
k_1K_{AcH}	0.0267	0.0331	0.0415	0.0515	
E_a					26.8

Table 4. Rate parameters for C_4 products formation from AcH-EtOH conversion over La-DeAlBEA

Rate parameter		K_E	K_Y	k_Y
T, K	**563**	0.37	0.35	0.31
	573	0.30	0.29	0.45
	593	0.22	0.17	0.80
Enthalpy (kJ/mol)	**EtOH adsorption ΔH_{ads} (EtOH)**	-47.5		
	AcH-EtOH co-adsorption ΔH_{ads} (AcH-EtOH)		-67.9	
	Intrinsic E_a (kJ/mol)			86.9

Conclusions

An investigation was conducted of the reaction mechanism and kinetics of EtOH and AcH conversion to 1,3-BD over isolated La Lewis acid sites grafted into the silanol nests of dealuminated Beta zeolite. La-DeAlBEA prepared with La/Al < 0.24 characterized by IR spectroscopy of adsorbed pyridine, deuterated acetonitrile, and DTBPy and XAS reveals that La is present as isolated sites with a structure of $(\equiv SiO)_2La{-}OH{\cdots}HO{-}Si\equiv$, a structure containing both Lewis acidic La sites and weak Brønsted acidic sites. On the other hand, isolated La sites grafted onto the isolated silanol groups over SiO_2 are present only in the form of $(\equiv SiO)_2La{-}OH$, with no evidence that La-OH groups are H-bonded with adjacent Si-OH groups. Investigation of the mechanism and kinetics of AcH coupling over isolated La-DeAlBEA shows that Lewis acid La sites catalyze C-C coupling and MPV hydrogen transfer, whereas weakly Brønsted acid sites associated with $\equiv SiOH$ groups interacting with La Lewis acid sites and unconsumed silanol nests contribute to

dehydration of crotyl alcohol. It is notable that isolated La sites on both La-DeAlBEA and La-SiO_2 exhibit similar AcH aldol condensation rates, supporting the conclusion that La Lewis acid sites catalyze C-C coupling. An increase in the rate of 1,3-BD formation by a factor of 4.8 was observed upon addition of EtOH to AcH fed over La-DeAlBEA, whereas the rate of C_4 product formation over La-SiO_2 was not affected by the addition of EtOH. Combined with the similar chemical structure of La sites for both La-DeAlBEA and La-SiO_2, this difference in catalytic behavior is ascribed to the presence of H-bonding interaction between La-OH groups and proximal silanol groups in La-DeAlBEA. The rate of crotonaldehyde formation via AcH aldol condensation over La-DeAlBEA exhibits close to first order dependence on AcH partial pressure, suggesting that the enolization of AcH is the most likely rate-limiting step in aldol condensation In the case of EtOH-AcH conversion to 1,3-BD, both EtOH and AcH exhibit a positive order dependence, implying that both EtOH and AcH are involved in the new C-C bond formation pathway. The results of this work provide critical insight for the development of active catalysts for the conversion of EtOH to 1.3-BD.

Associated content

Author information

Corresponding Author

Alexis T. Bell – *Chemical Sciences Division, Lawrence Berkeley National Laboratory, Berkeley, California 94720, United States; Department of Chemical and Biomolecular Engineering, University of California, Berkeley, Berkeley, California 94720, United States;* orcid.org/0000-0002-5738-4645; Email: alexbell@berkeley.edu

Authors

Yanfei Zhang – *Green Shipping and Carbon Neutrality Lab, College of Environmental Science and Engineering, Dalian Maritime University, Dalian 116026, China; Chemical Sciences Division, Lawrence Berkeley National Laboratory, Berkeley, California 94720, United States; National Engineering*

Laboratory for Methanol to Olefins, Dalian National Laboratory for Clean Energy, Dalian Institute of Chemical Physics, Chinese Academy of Sciences, Dalian 116023, China; Department of Chemical and Biomolecular Engineering, University of California, Berkeley, Berkeley, California 94720, United States

Liang Qi – *National Engineering Laboratory for Methanol to Olefins, Dalian National Laboratory for Clean Energy, Dalian Institute of Chemical Physics, Chinese Academy of Sciences, Dalian 116023, China; Chemical Sciences Division, Lawrence Berkeley National Laboratory, Berkeley, California 94720, United States; Department of Chemical and Biomolecular Engineering, University of California, Berkeley, Berkeley, California 94720, United States*

Yuting Li – *U.S. DOE Ames National Laboratory, Iowa State University, Ames, Iowa 50011, United States*

Tingshu Yang – *Green Shipping and Carbon Neutrality Lab, College of Environmental Science and Engineering, Dalian Maritime University, Dalian 116026, China*

Debora M. Meira – *Canadian Light Source, 44 Innovation Blvd., Saskatoon, Saskatchewan S7N 2V3, Canada*

Chaochao Dun – *The Molecular Foundry, Lawrence Berkeley National Laboratory, Berkeley, CA, 94720, United States*

Haocheng Hu – *National Engineering Laboratory for Methanol to Olefins, Dalian National Laboratory for Clean Energy, Dalian Institute of Chemical Physics, Chinese Academy of Sciences, Dalian 116023, China*

Huihui Chen – *National Engineering Laboratory for Methanol to Olefins, Dalian National Laboratory for Clean Energy, Dalian Institute of Chemical Physics, Chinese Academy of Sciences, Dalian 116023, China*

Shutao Xu – *National Engineering Laboratory for Methanol to Olefins, Dalian National Laboratory for Clean Energy, Dalian Institute of Chemical Physics, Chinese Academy of Sciences, Dalian 116023, China*

Jeffrey J. Urban – *The Molecular Foundry, Lawrence Berkeley National Laboratory, Berkeley, CA, 94720, United States*

Aaron D. Sadow – *U.S. DOE Ames National Laboratory and Department of Chemistry, Iowa State University, Ames, Iowa 50011, United States*

Takeshi Kobayashi – *U.S. DOE Ames National Laboratory, Iowa State University, Ames, Iowa 50011, United States*

Long Qi – *U.S. DOE Ames National Laboratory, Iowa State University, Ames, Iowa 50011, United States*

Peng Tian– *National Engineering Laboratory for Methanol to Olefins, Dalian National Laboratory for Clean Energy, Dalian Institute of Chemical Physics, Chinese Academy of Sciences, Dalian 116023, China*

Authors contributions

Y. Z. and L. Q. contributed equally.

Notes

The authors declare no competing financial interest.

Supporting Information

Experimental methods; IR result of dealumination of H-BEA (Figure S1); ICP and XRD results of La-DeAlBEA (Figures S2, S3); plots of integrated peak area for pyridine adsorption bands versus La/Al ratio for La-DeAlBEA (Figure S4), changes of IR spectra for CD_3CN and pyridine adsorption with purging time (Figures S5, S6); 1H NMR spectra and spectral deconvolution (Figure S7, Table S2); changes of k-space and R-space data before and after MEE removal treatment of 0.06La-DeAlBEA and 0.85wt%La-SiO_2 (Figures S8, S9); formation rates of C_4 products with TOS over La-SiO_2 (Figure S10); space time investigation of AcH aldol condensation and ethanol-AcH conversion (Figure S11); derivation of the expressions of the rates of C_4 products formation from AcH aldol condensation.

Acknowledgement

This work was supported by the Office of Science, Office of Basic Energy Sciences, of the U.S. Department of Energy (DOE) under Contract No. DE-AC02-05CH11231 and the National Natural Science Foundation of China (No. 22302025). P. T. acknowledge support by the National Natural Science Foundation of China (No. 21991090, 21991091). C.D. and J.J.U. also acknowledge support for their contributions to this work by the Office of Science, Office of Basic Energy Sciences, of the U.S. Department of Energy, under Contract No. DE-AC02-05CH11231. Y. Z. also thank Dr. Guangying Fu for help with IR measurements and supported by the Fundamental Research Funds for the Central Universities of Dalian Maritime University in China (No. 3132023520). Y.L., T.K., A.D.S., and L.Q. are supported by the U.S. Department of Energy (DOE), Office of Basic Energy Sciences, Division of Chemical Sciences, Geosciences, and Biosciences, Catalysis Science program. The Ames National Laboratory is operated for the U.S. DOE by Iowa State University under Contract No. DE-AC02-07CH11358. This research used the Advanced Photon Source resources, an Office of Science User Facility operated by Argonne National Laboratory for the U.S. Department of Energy (DOE) Office of Science. The U.S. DOE supported it under Contract No. DE-AC02-06CH11357, and the Canadian Light Source and its funding partners.

References

1. Makshina, E. V.; Dusselier, M.; Janssens, W.; Degreve, J.; Jacobs, P. A.; Sels, B. F., Review of old chemistry and new catalytic advances in the on-purpose synthesis of butadiene. *Chem. Soc. Rev.* **2014,** *43*, 7917-7953.
2. Dussol, D.; Cadran, N.; Laloue, N.; Renaudot, L.; Schweitzer, J.-M., New insights of butadiene production from ethanol: Elucidation of concurrent reaction pathways and kinetic study. *Chem. Eng. J.* **2020,** *391*, 123586.
3. Qi, L.; Zhang, Y.; Conrad, M. A.; Russell, C. K.; Miller, J.; Bell, A. T., Ethanol conversion to butadiene over isolated zinc and yttrium sites grafted onto dealuminated beta zeolite. *J. Am. Chem. Soc.* **2020,** *142* 14674-14687.
4. Sushkevich, V. L.; Ivanova, I. I., Mechanistic study of ethanol conversion into butadiene over silver promoted zirconia catalysts. *Appl. Catal. B: Environ.* **2017,** *215*, 36-49.
5. White, W. C., Butadiene production process overview. *Chem.-Biol. Interact.* **2007,** *166*, 10-14.

6. Zhang, Y.; Qi, L.; Leonhardt, B.; Bell, A. T., Mechanism and kinetics of n-butane dehydrogenation to 1, 3-butadiene catalyzed by isolated Pt sites grafted onto ≡ SiOZn–OH nests in dealuminated zeolite Beta. *ACS Catal.* **2022,** *12*, 3333-3345.
7. Pomalaza, G.; Ponton, P. A.; Capron, M.; Dumeignil, F., Ethanol-to-butadiene: the reaction and its catalysts. *Catal. Sci. Technol.* **2020,** *10*, 4860-4911.
8. Shylesh, S.; Gokhale, A. A.; Scown, C. D.; Kim, D.; Ho, C. R.; Bell, A. T., From sugars to wheels: The conversion of ethanol to 1,3-butadiene over metal-promoted magnesia-silicate catalysts. *ChemSuschem* **2016,** *9*, 1462-1472.
9. Pomalaza, G.; Capron, M.; Ordomsky, V.; Dumeignil, F., Recent breakthroughs in the conversion of ethanol to butadiene. *Catalysts* **2016,** *6*, 203.
10. Ho, C. R.; Shylesh, S.; Bell, A. T., Mechanism and kinetics of ethanol coupling to butanol over hydroxyapatite. *ACS Catal.* **2016,** *6*, 939-948.
11. Sun, J.; Wang, Y., Recent advances in catalytic conversion of ethanol to chemicals. *ACS Catal.* **2014,** *4*, 1078-1090.
12. Li, J.; Cheng, W., Comparison of life-cycle energy consumption, carbon emissions and economic costs of coal to ethanol and bioethanol. *Appl. Energy* **2020,** *277*, 115574.
13. Xu, X.; Liu, Y.; Zhang, F.; Di, W.; Zhang, Y., Clean coal technologies in China based on methanol platform. *Catal. Today* **2017,** *298*, 61-68.
14. Yan, T. T.; Dai, W. L.; Wu, G. J.; Lang, S.; Hunger, M.; Guan, N. J.; Li, L. D., Mechanistic insights into one-step catalytic conversion of ethanol to butadiene over bifunctional Zn-Y/Beta zeolite. *ACS Catal.* **2018,** *8*, 2760-2773.
15. Mamedov, K.; Davis, R. J., Cascade reaction of ethanol to butadiene over Ag-promoted, silica or zeolite-supported Ta, Y, Pr, or La oxide catalysts. *ACS Catal.* **2023,** *13*, 3333-3344.
16. Shylesh, S.; Kim, D.; Gokhale, A. A.; Canlas, C. G.; Struppe, J. O.; Ho, C. R.; Jadhav, D.; Yeh, A.; Bell, A. T., Effects of composition and structure of Mg/Al oxides on their activity and selectivity for the condensation of methyl ketones. *Ind. Eng. Chem. Res.* **2016,** *55*, 10635-10644.
17. Palagin, D.; Sushkevich, V. L.; Ivanova, I. I., C-C coupling catalyzed by zeolites: Is enolization the only possible pathway for aldol condensation? *J. Phys. Chem. C.* **2016,** *120*, 23566-23575.
18. Sushkevich, V. L.; Palagin, D.; Ivanova, I. I., With open arms: Open sites of ZrBEA zeolite facilitate selective synthesis of butadiene from ethanol. *ACS Catal.* **2015,** *5*, 4833-4836.
19. Chieregato, A.; Ochoa, J. V.; Bandinelli, C.; Fornasari, G.; Cavani, F.; Mella, M., On the chemistry of ethanol on basic oxides: Revising mechanisms and intermediates in the Lebedev and Guerbet reactions. *ChemSuschem* **2015,** *8*, 377-388.
20. Larina, O.; Kyriienko, P.; Soloviev, S., Effect of lanthanum in Zn-La (-Zr)-Si oxide compositions on their activity in the conversion of ethanol into 1, 3-butadiene. *Theor. Exp. Chem.* **2016,** *52*, 51-56.
21. Dai, W. L.; Zhang, S. S.; Yu, Z. Y.; Yan, T. T.; Wu, G. J.; Guan, N. J.; Li, L. D., Zeolite structural confinement effects enhance one-pot catalytic conversion of ethanol to butadiene. *ACS Catal.* **2017,** *7*, 3703-3706.

22. Pomalaza, G.; Vofo, G.; Capron, M.; Dumeignil, F., ZnTa-TUD-1 as an easily prepared, highly efficient catalyst for the selective conversion of ethanol to 1,3-butadiene. *Green Chem.* **2018,** *20*, 3203-3209.
23. Cheong, J. L.; Shao, Y. L.; Tan, S. J. R.; Li, X. K.; Zhang, Y. G.; Lee, S. S., Highly active and selective Zr/MCF catalyst for production of 1,3-butadiene from ethanol in a dual fixed bed reactor system. *ACS Sustain. Chem. Eng.* **2016,** *4*, 4887-4894.
24. De Baerdemaeker, T.; Feyen, M.; Muller, U.; Yilmaz, B.; Xiao, F. S.; Zhang, W. P.; Yokoi, T.; Bao, X. H.; Gies, H.; De Vos, D. E., Bimetallic Zn and Hf on silica catalysts for the conversion of ethanol to 1,3-butadiene. *ACS Catal.* **2015,** *5*, 3393-3397.
25. Wang, C.; Zheng, M. Y.; Li, X. S.; Li, X. Q.; Zhang, T., Catalytic conversion of ethanol into butadiene over high performance LiZnHf-MFI zeolite nanosheets. *Green Chem.* **2019,** *21*, 1006-1010.
26. Han, Z.; Li, X.; Zhang, M.; Liu, Z.; Gao, M., Sol–gel synthesis of ZrO_2–SiO_2 catalysts for the transformation of bioethanol and acetaldehyde into 1, 3-butadiene. *RSC Adv.* **2015,** *5*, 103982-103988.
27. Li, H.; Pang, J.; Jaegers, N. R.; Kovarik, L.; Engelhard, M.; Savoy, A. W.; Hu, J.; Sun, J.; Wang, Y., Conversion of ethanol to 1, 3–butadiene over Ag–ZrO_2/SiO_2 catalysts: The role of surface interfaces. *J. Energy Chem.* **2021,** *54*, 7-15.
28. Kyriienko, P. I.; Larina, O. V.; Popovych, N. O.; Soloviev, S. O.; Millot, Y.; Dzwigaj, S., Effect of the niobium state on the properties of NbSiBEA as bifunctional catalysts for gas-and liquid-phase tandem processes. *J. Mol. Catal. A: Chem.* **2016,** *424*, 27-36.
29. Corson, B.; Jones, H.; Welling, C.; Hinckley, J.; Stahly, E., Butadiene from ethyl alcohol. Catalysis in the one-and two-step processes. *Ind. Eng. Chem.* **1950,** *42*, 359-373.
30. Kim, T.-W.; Kim, J.-W.; Kim, S.-Y.; Chae, H.-J.; Kim, J.-R.; Jeong, S.-Y.; Kim, C.-U., Butadiene production from bioethanol and acetaldehyde over tantalum oxide-supported spherical silica catalysts for circulating fluidized bed. *Chem. Eng. J.* **2015,** *278*, 217-223.
31. Larina, O. V.; Shcherban, N. D.; Kyriienko, P. I.; Remezovskyi, I. M.; Yaremov, P. S.; Khalakhan, I.; Mali, G.; Soloviev, S. O.; Orlyk, S. M.; Dzwigaj, S., Design of effective catalysts based on ZnLaZrSi oxide systems for obtaining 1, 3-butadiene from aqueous ethanol. *ACS Sustain. Chem. Eng.* **2020,** *8*, 16600-16611.
32. Zhang, J.; Wegener, E. C.; Samad, N. R.; Harris, J. W.; Unocic, K. A.; Allard, L. F.; Purdy, S.; Adhikari, S.; Cordon, M. J.; Miller, J. T., Isolated metal sites in Cu–Zn–Y/Beta for direct and selective butene-rich C_{3+} olefin formation from ethanol. *ACS Catal.* **2021,** *11*, 9885-9897.
33. Sushkevich, V. L.; Ivanova, I. I.; Taarning, E., Ethanol conversion into butadiene over Zr-containing molecular sieves doped with silver. *Green Chem.* **2015,** *17*, 2552-2559.
34. Zhang, Y.; Qi, L.; Lund, A.; Lu, P.; Bell, A. T., Mechanism and kinetics of acetone conversion to isobutene over isolated Hf sites grafted to Silicalite-1 and SiO_2.

J. Am. Chem. Soc. **2021,** *143*, 8352-8366.
35. Kyriienko, P. I.; Larina, O. V.; Soloviev, S. O.; Orlyk, S. M.; Dzwigaj, S., High selectivity of TaSiBEA zeolite catalysts in 1, 3-butadiene production from ethanol and acetaldehyde mixture. *Catal. Commun.* **2016,** *77*, 123-126.
36. Harris, J. W.; Cordon, M. J.; Di Iorio, J. R.; Vega-Vila, J. C.; Ribeiro, F. H.; Gounder, R., Titration and quantification of open and closed Lewis acid sites in Sn-Beta zeolites that catalyze glucose isomerization. *J. Catal.* **2016,** *335*, 141-154.
37. Kurmach, M. M.; Larina, O. V.; Kyriienko, P. I.; Yaremov, P. S.; Trachevsky, V. V.; Shvets, O. V.; Soloviev, S. O., Hierarchical Zr-MTW zeolites doped with copper as catalysts of ethanol conversion into 1,3-butadiene. *ChemistrySelect* **2018,** *3*, 8539-8546.
38. Müller, P.; Burt, S. P.; Love, A. M.; McDermott, W. P.; Wolf, P.; Hermans, I., Mechanistic study on the Lewis acid catalyzed synthesis of 1, 3-butadiene over Ta-BEA using modulated operando DRIFTS-MS. *ACS Catal.* **2016,** *6*, 6823-6832.
39. Sushkevich, V. L.; Vimont, A.; Travert, A.; Ivanova, I. I., Spectroscopic evidence for open and closed Lewis acid sites in ZrBEA zeolites. *J. Phys. Chem. C* **2015,** *119*, 17633-17639.
40. Borate, S. N.; Purdy, S. C.; Zhang, J.; Bornes, C.; Cordon, M. J.; Li, M.; Mafra, L.; Sutton, A. D.; Li, Z.; Harris, J. W., Quantification of active sites in yttrium containing dealuminated Beta zeolites during conversion of ethanol and acetaldehyde to butadiene. *J. Catal.* **2024**, *433*,115468.
41. Dijkmans, J.; Gabriëls, D.; Dusselier, M.; de Clippel, F.; Vanelderen, P.; Houthoofd, K.; Malfliet, A.; Pontikes, Y.; Sels, B. F., Productive sugar isomerization with highly active Sn in dealuminated β zeolites. *Green Chem.* **2013,** *15*, 2777-2785.
42. Tang, B.; Dai, W.; Wu, G.; Guan, N.; Li, L.; Hunger, M., Improved postsynthesis strategy to Sn-Beta zeolites as Lewis acid catalysts for the ring-opening hydration of epoxides. *ACS Catal.* **2014,** *4*, 2801-2810.
43. Nogier, J.-P.; Millot, Y.; Man, P. P.; Shishido, T.; Che, M.; Dzwigaj, S., Probing the incorporation of Ti (IV) into the BEA Zeolite Framework by XRD, FTIR, NMR, and DR UV− jp810722bis. *J. Phys. Chem. C* **2009,** *113*, 4885-4889.
44. Qi, L.; Babucci, M.; Zhang, Y.; Lund, A.; Liu, L.; Li, J.; Chen, Y.; Hoffman, A. S.; Bare, S. R.; Han, Y.; Gates, B. C.; Bell, A. T., Propane dehydrogenation catalyzed by isolated Pt atoms in ≡SiOZn–OH nests in dealuminated zeolite Beta. *J. Am. Chem. Soc.* **2021,** *143*, 21364-21378.
45. Nozik, D.; Tinga, F. M. P.; Bell, A. T., Propane dehydrogenation and cracking over Zn/H-MFI prepared by solid-state ion exchange of $ZnCl_2$. *ACS Catal.* **2021,** *11*, 14489-14506.
46. Dzwigaj, S.; Janas, J.; Gurgul, J.; Socha, R. P.; Shishido, T.; Che, M., Do Cu (II) ions need Al atoms in their environment to make CuSiBEA active in the SCR of NO by ethanol or propane? A spectroscopy and catalysis study. *Appl. Catal. B-Environ.* **2009,** *85*, 131-138.
47. Hanukovich, S.; Dang, A.; Christopher, P., Influence of metal oxide support acid sites on Cu-catalyzed nonoxidative dehydrogenation of ethanol to acetaldehyde. *ACS Catal.* **2019,** *9*, 3537-3550.

48. Sushkevich, V. L.; Ivanova, I. I.; Yakimov, A. V., Revisiting acidity of SnBEA catalysts by combined application of FTIR spectroscopy of different probe molecules. *J. Phys. Chem. C* **2017,** *121* 11437-11447.
49. Paze, C.; Zecchina, A.; Spera, S.; Spano, G.; Rivetti, F., Acetonitrile as probe molecule for an integrated ^{1}H NMR and FTIR study of zeolitic Brønsted acidity: Interaction with zeolites H-ferrierite and H-beta. *Phys. Chem. Chem. Phys.* **2000,** *2*, 5756-5760.
50. Wichterlová, B.; Tvarůžková, Z.; Sobalık, Z.; Sarv, P., Determination and properties of acid sites in H-ferrierite: A comparison of ferrierite and MFI structures. *Micropor. Mesopor. Mat.* **1998,** *24*, 223-233.
51. Boronat, M.; Concepción, P.; Corma, A.; Navarro, M. T.; Renz, M.; Valencia, S., Reactivity in the confined spaces of zeolites: the interplay between spectroscopy and theory to develop structure–activity relationships for catalysis. *Phys. Chem. Chem. Phys.* **2009,** *11*, 2876-2884.
52. Pelmenschikov, A.; Van Santen, R.; Janchen, J.; Meijer, E., Acetonitrile-d3 as a probe of Lewis and Brønsted acidity of zeolites. *J. Phys. Chem.* **1993,** *97*, 11071-11074.
53. Yang, G.; Lan, X.; Zhuang, J.; Ma, D.; Zhou, L.; Liu, X.; Han, X.; Bao, X., Acidity and defect sites in titanium silicalite catalyst. *Appl. Catal. A-Gen.* **2008,** *337*, 58-65.
54. Yang, G.; Zhou, L.; Han, X., Lewis and Brönsted acidic sites in M^{4+}-doped zeolites (M= Ti, Zr, Ge, Sn, Pb) as well as interactions with probe molecules: A DFT study. *J.Mol. Catal. A-Chem.* **2012,** *363*, 371-379.
55. Corma, A.; Fornes, V.; Forni, L.; Marquez, F.; Martınez-Triguero, J.; Moscotti, D., 2, 6-Di-tert-butyl-pyridine as a probe molecule to measure external acidity of zeolites. *J. Catal.* **1998,** *179*, 451-458.
56. Kots, P. A.; Zabilska, A. V.; Ivanova, I. I., Selective self-condensation of butanal over Zr-BEA zeolites. *ChemCatchem* **2020,** *12*, 248-258.
57. Hunger, M.; Ernst, S.; Steuernagel, S.; Weitkamp, J., High-field ^{1}H MAS NMR investigations of acidic and non-acidic hydroxyl groups in zeolites H-Beta, H-ZSM-5, H-ZSM-58 and H-MCM-22. *Micropor. Mat.* **1996,** *6*, 349-353.
58. Huang, J.; Jiang, Y.; Marthala, V. R.; Ooi, Y. S.; Weitkamp, J.; Hunger, M., Concentration and acid strength of hydroxyl groups in zeolites La, Na-X and La, Na-Y with different lanthanum exchange degrees studied by solid-state NMR spectroscopy. *Micropor. Mesopor. Mat.* **2007**, *104*, 129-136.57.
59. The Materials, Materials Data on La by Materials Project. United States, 2020.
60. The Materials, Materials Data on La_2O_3 by Materials Project. United States, 2020.
61. Smerigan, A.; Biswas, S.; Vila, F. D.; Hong, J.; Perez-Aguilar, J.; Hoffman, A. S.; Greenlee, L.; Getman, R. B.; Bare, S. R., Aqueous structure of Lanthanide-EDTA coordination complexes determined by a combined DFT/EXAFS approach. *Inorg. Chem.* **2023,** *62*, 14523-14532.
62. Stamberga, D.; Healy, M. R.; Bryantsev, V. S.; Albisser, C.; Karslyan, Y.; Reinhart, B.; Paulenova, A.; Foster, M.; Popovs, I.; Lyon, K.; Moyer, B. A.; Jansone-Popova, S., Structure activity relationship approach toward the improved

separation of rare-earth elements using diglycolamides. *Inorg. Chem.* **2020,** *59*, 17620-17630.
63. Chaboy, J.; Marcelli, A.; Tyson, T. A., Influence of double-electron transitions on the EXAFS L edges of rare-earth systems. *Phys. Rev. B Condens. Matter* **1994,** *49*, 11652-11661.
64. The Materials Project for La_2O_3 (mp-2292) from database version v2023.11.1. http://next-gen.materialsproject.org/materials/mp-2292 (accessed May 8, 2024).
65. D'Angelo, P.; Zitolo, A.; Migliorati, V.; Chillemi, G.; Duvail, M.; Vitorge, P.; Abadie, S.; Spezia, R., Revised ionic radii of lanthanoid(III) ions in aqueous solution. *Inorg. Chem.* **2011,** *50,* 4572-4579.
66. Yan, T. T.; Yang, L.; Dai, W. L.; Wang, C. M.; Wu, G. J.; Guan, N. J.; Hunger, M.; Li, L. D., On the deactivation mechanism of zeolite catalyst in ethanol to butadiene conversion. *J. Catal.* **2018,** *367*, 7-15. 65.
67. Sushkevich, V. L.; Vimont, A.; Travert, A.; Ivanova, I. I., Spectroscopic Evidence for Open and Closed Lewis Acid Sites in ZrBEA Zeolites. *J. Phys. Chem. C* **2015,** *119*, 17633-17639.
68. Hanna, D. G.; Shylesh, S.; Li, Y.-P.; Krishna, S.; Head-Gordon, M.; Bell, A. T., Experimental and theoretical study of n-butanal self-condensation over Ti species supported on silica. *ACS Catal.* **2014,** *4*, 2908-2916.
69. Yan, T. T.; Yao, S. K.; Dai, W. L.; Wu, G. J.; Guan, N. J.; Li, L. D., Self-aldol condensation of aldehydes over Lewis acidic rare-earth cations stabilized by zeolites. *Chinese J. Catal.* **2021,** *42*, 595-605.

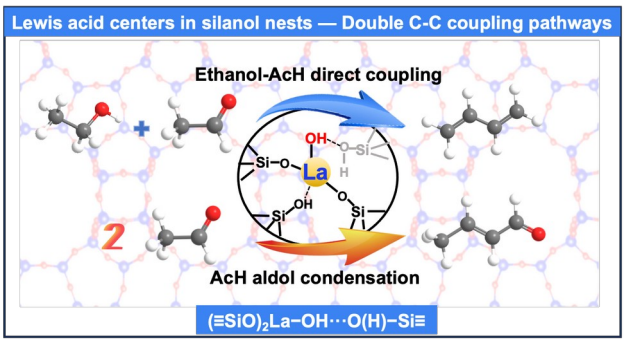
Lewis acid centers in silanol nests — Double C-C coupling pathways
Ethanol-AcH direct coupling
OH
Si
O
H
Si–O
La
O
Si
OH
Si
2
AcH aldol condensation
(≡SiO)2La–OH···O(H)–Si≡